A Look at the Surface-Based Temperature Inversion on the Antarctic Plateau

STEPHEN R. HUDSON AND RICHARD E. BRANDT

Department of Atmospheric Sciences, University of Washington, Seattle, Washington

(Manuscript received 25 June 2004, in final form 2 November 2004)

ABSTRACT

Data from radiosondes, towers, and a thermistor string are used to characterize the temperature inversion at two stations: the Amundsen-Scott Station at the South Pole, and the somewhat higher and colder Dome C Station at a lower latitude.

Ten years of temperature data from a 22-m tower at the South Pole are analyzed. The data include 2- and 22-m temperatures for the entire period and 13-m temperatures for the last 2 yr. Statistics of the individual temperatures and the differences among the three levels are presented for summer (December and January) and winter (April–September).

The relationships of temperature and inversion strength in the lowest 22 m with wind speed and downward longwave flux are examined for the winter months. Two preferred regimes, one warming and one cooling, are found in the temperature versus longwave flux data, but the physical causes of these regimes have not been determined. The minimum temperatures and the maximum inversions tend to occur not with calm winds, but with winds of 3–5 m s^{-1}, likely due to the inversion wind. This inversion wind also explains why the near-surface winds at South Pole blow almost exclusively from the northeast quadrant.

Temperature data from the surface to 2 m above the surface from South Pole in the winter of 2001 are presented, showing that the steepest temperature gradient in the entire atmosphere is in the lowest 20 cm. The median difference between the temperatures at 2 m and the surface is over 1.0 K in winter; under clear skies this difference increases to about 1.3 K.

Monthly mean temperature profiles of the lowest 30 km of the atmosphere over South Pole are presented, based on 10 yr of radiosonde data. These profiles show large variations in lower-stratospheric temperatures, and in the strength and depth of the surface-based inversion.

The near-destruction of a strong inversion at South Pole during 7 h on 8 September 1992 is examined using a thermal-conductivity model of the snowpack, driven by the measured downward longwave flux. The downward flux increased when a cloud moved over the station, and it seems that this increase in radiation alone can explain the magnitude and timing of the warming near the surface.

Temperature data from the 2003/04 and 2004/05 summers at Dome C Station are presented to show the effects of the diurnal cycle of solar elevation over the Antarctic Plateau. These data include surface temperature and 2- and 30-m air temperatures, as well as radiosonde air temperatures. They show that strong inversions, averaging 10 K between the surface and 30 m, develop quickly at night when the sun is low in the sky, but are destroyed during the middle of the day. The diurnal temperature range at the surface was 13 K, but only 3 K at 30 m.

1. Introduction

It has been known for decades that a surface-based temperature inversion exists over the Antarctic Plateau and that its existence is not only a major feature of this region's climate, but also a driver of some aspects of its climate, including near-surface winds and atmospheric radiation. A significant inversion exists at the surface of the Antarctic Plateau in every month but December and January (e.g., Schwerdtfeger 1970a).

The inversion exists because the snow-surface emissivity is greater than the atmospheric emissivity. When the energy absorbed at the surface from solar radiation is small, this inequality in emissivities results in a temperature inversion.

Given that the sum of sensible, latent, and subsurface heat fluxes provides only about 10%–15% of the energy the surface emits in winter (Schlatter 1972; Carroll 1982) and that the surface temperature is nearly con-

Corresponding author address: Stephen R. Hudson, Department of Atmospheric Sciences, University of Washington, Box 351640, Seattle, WA 98195-1640.
E-mail: hudson@atmos.washington.edu

stant during the 6-month winter (Schwerdtfeger 1984), we can see that the upward longwave emission by the surface must be nearly balanced by the downward longwave radiation reaching the surface from the atmosphere. This implies that, in winter,

$$0.85\,\varepsilon_s \sigma T_s^4 \approx \varepsilon_a \sigma T_a^4, \quad (1)$$

where $\varepsilon_s \approx 1.0$ is the snow-surface emissivity, ε_a is the effective emissivity of the atmosphere, $\sigma = 5.6696 \times 10^{-8}$ W m^{-2} K^{-4} is the Stefan–Boltzmann constant, T_s is the surface temperature, and T_a is the effective temperature of the atmosphere (i.e., at levels where most of the emission originates); the factor 0.85 comes from the fact that about 15% of the energy emitted by the surface is replenished by nonradiative mechanisms. Therefore, in winter, $(T_s/T_a) \approx (\varepsilon_a/0.85)^{0.25}$, so the surface temperature will have to be lower than the air temperature so long as the emissivity of the atmosphere is less than 0.85, a criterion violated only under optically thick clouds. For a typical wintertime inversion, with $T_s = 213$ K and $T_a = 233$ K, Eq. (1) implies $\varepsilon_a \approx 0.6$.

The inversion is of interest to researchers in a variety of fields. Waddington and Morse (1994) and Van Lipzig et al. (2002) showed that the inversion can affect ice-core records, and therefore must be considered for proper retrieval of paleoclimate from ice cores. The ability of inversion layers to resist vertical mixing affects atmospheric boundary layer chemistry and snow chemistry (Harder et al. 2000; Davis et al. 2001). One of the rapidly growing fields of research on the Antarctic Plateau is ground-based astronomy, which can benefit from the high elevation and cold, dry atmosphere. However, Marks (2002) and Travouillon et al. (2003) showed that the presence of strong temperature gradients in the inversion layer can hinder atmospheric "seeing," while its shallow depth allows for good use of adaptive optics. Significant temperature gradients in the lowest 2 m of the atmosphere associated with the inversion mean that satellite retrievals of surface temperature in Antarctica will be lower than the "surface" air temperature measured at a station, which is usually measured around 2 m above the surface.

Many studies of the inversion have tried to examine it through radiosonde data. Among others, these have resulted in an analysis of the relationship between near-surface winds and the inversion by Dalrymple et al. (1966) and Lettau and Schwerdtfeger (1967) and in a climatology of inversion strength across the continent by Phillpot and Zillman (1970), which showed that inversions over South Pole average about 20 K in winter, and those over the highest parts of the plateau average over 25 K. Given the very rapid increase of temperature with height in these inversions (Schwerdtfeger 1984) these radiosondes may not adequately capture the details of the inversion near the surface (Mahesh et al. 1997).

More recently, Connolley (1996) compared the climatology produced by Phillpot and Zillman with that produced by the Met Office Unified Model, a global climate model. Connolley's results are similar to those of Phillpot and Zillman, but show a dependence of inversion strength on terrain slope, which was not included by Phillpot and Zillman. This approach is useful in that it can help to fill in the many data voids that exist over large portions of Antarctica. On the other hand, we are a long way from being able to replace observations with model results.

Towers have been used to study the inversion as well; these have the benefit of allowing for more accurate measurements to be made in the lowest portion of the atmosphere, where the inversion is most pronounced. Perhaps the best-known tower-based study of the Antarctic Plateau boundary layer was conducted at Plateau Station, where temperatures and winds were measured at numerous levels on a 32-m tower (Riordan 1977). Dalrymple et al. (1966) also presented data collected on an 8-m tower at South Pole in 1958.

This paper presents data collected at South Pole from radiosondes and from a 22-m tower over a 10-yr period. For most of the period the ground-based data include only 2- and 22-m temperatures, along with 10-m wind and downward infrared flux, but some interesting features of the inversion can still be examined with this limited dataset. Data from a string of thermistors between the surface and 2 m that was operated during the winter of 2001 are used to examine the inversion very near the surface at South Pole. The larger-scale characteristics of the inversion are captured in the radiosonde data. Additionally, some comparisons are made to tower-based and radiosonde data collected in the summers of 2003/04 and 2004/05 at Dome C, where a significant diurnal cycle is observed.

The aim of this paper is to present an overview of the temperature profile over the Antarctic Plateau at different scales, with particular focus on the structure of the surface-based temperature inversion and on some of the factors that influence this inversion. The use of 10 yr of both radiosonde and tower-based data from South Pole allows for analyses of the temperature profile that come closer to an actual climatology than previous works. The longer period of record also allows for more robust analyses of the relationships between the inversion and the winds and downward longwave radiation, which are believed to influence the inversion. The data from the surface to 2 m, while less climatologically ro-

bust, allow for the presentation of the character of the temperature profile at these very lowest levels.

The limited data from Dome C, in addition to being the first analysis of the inversion in that area of the plateau, give us a sense of how important the diurnal cycle is at lower-latitude sites on the Antarctic Plateau. While the character of the inversion over most of the plateau is likely similar to that at South Pole during winter months, these data will show that during months with significant sunlight the inversion at more northerly locations can differ dramatically from what is seen at South Pole.

This analysis should allow researchers in fields that are affected by the inversion to better understand its structure, and therefore how it will affect their data. It also presents a baseline against which models can be tested, for their ability to simulate both the mean conditions and the relationships between the inversion and winds and longwave fluxes.

The next section discusses the data used in this paper, and section 3 presents the temperature and inversion statistics at South Pole and discusses their relationships with winds and downward longwave flux. A case study of the destruction of a strong inversion is presented in section 4, and section 5 shows the diurnal cycle at Dome C. A summary is given in section 6.

2. Data

Data were obtained from two operational agencies as well as from three field projects of the University of Washington and one of the University of Idaho. The two locations where data were collected, South Pole and Dome C, are shown on the map in Fig. 1.

Most of the ground-based South Pole data presented here were collected by the National Oceanographic and Atmospheric Administration's Climate Monitoring and Diagnostics Laboratory (CMDL) at Amundsen-Scott South Pole Station. The air temperature and wind data are collected on a 22-m tower, and the downwelling longwave fluxes on the top of the building where CMDL operates, about 50 m from the tower. Both the tower and the building are in the Clean-Air Sector, in the normal upwind direction from the rest of the station. The temperatures are measured with aspirated platinum resistance probes, calibrated and intercompared annually, and with an accuracy of ± 0.1 K. The instruments are raised once each summer to maintain their nominal heights above the snow surface, because the snow accumulation in the vicinity of the tower is about 20 cm yr^{-1}. Wind data are collected using an R. M. Young model 05103 anemometer; wind speeds have an accuracy of $\pm 2\%$ with a 1 m s^{-1} threshold, and the wind directions are accurate to $\pm 5^\circ$ at 1.5 m s^{-1}.

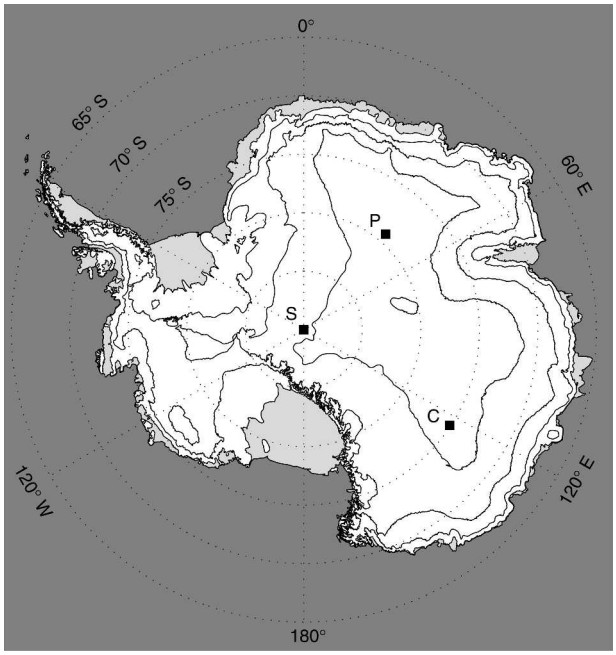

FIG. 1. A map of Antarctica showing the location of the stations mentioned in the text: South Pole is labeled with an "S," Plateau with a "P," and Dome C with a "C." Surface elevation is contoured at 1000-m intervals; the contour nearest South Pole and Dome C indicates an elevation of 3000 m.

The longwave flux data come from an Eppley PIR pyrgeometer, with an accuracy of ± 4 W m^{-2}.

These data include 1-min-resolution observations of the air temperature at 2 and 22 m for the period 19 January 1994–31 December 2003, as well as 13-m air temperatures from 14 January 2002–31 December 2003. They also include 1-min-resolution observations of wind speed and direction, measured at 10 m above the surface, from 19 January 1994–29 June 2003. The downward longwave flux data have 3-min resolution from 1994–97, and 1-min resolution from 1 January 1998–29 June 2003. Hourly temperature and wind data collected during earlier years (1987–93) were not used because some periods in this dataset showed obvious biases, and the data often did not compare well with those from the South Pole Meteorological Office.

Two other smaller sets of ground-based data from South Pole are also used. In section 3c temperature data from thermistors located at the surface and 0.2, 0.5, 1, and 2 m above the surface are presented. These data were collected just inside the Clean-Air Sector between 21 March and 21 September 2001 as part of the South Pole Atmospheric Radiation and Cloud Lidar Experiment (Walden et al. 2001). The five YSI 44033 thermistors were intercalibrated in a water–ice bath and in a dry ice and methanol mixture before the experiment and agreed to within ± 0.05 K. Data were col-

lected from all five thermistors every 5 min, and their heights were adjusted every 3 days during the winter.

The 11-m air temperature and downward longwave flux shown in section 4 were collected using an Eppley pyrgeometer with an attached thermistor at that height (Walden 1995).

The South Pole radiosonde data were collected by the South Pole Meteorological Office, currently operated by Raytheon Polar Services Corporation. The data were provided by the Antarctic Meteorological Research Center. Soundings from 1994–2003 were used. During the summer operational season, October–February, two soundings are normally conducted each day, at 0000 and 1200 UTC; during most of the rest of the year only the 0000 UTC sounding is made. These data were collected with Atmospheric Instrumentation Research Incorporated (AIR) model 4A radiosondes from 1994–96, with AIR model 5A sondes from 1997–July 2001, and with Vaisala RS80 and RS90 sondes from August 2001–December 2003. In addition to rejecting individual points containing values outside the range observed at South Pole ($T \leq -110$°C or $T \geq +10$°C, where T is the temperature at any height), a quality control check was done in which each sounding was briefly viewed as a temperature–height profile. Of the 4989 soundings obtained, 208 were removed because of problems found during this quality check, most because they were missing more than 150 m of data at the beginning of the sounding, or because they reported bad data in the lowest part of the sounding. In another 218 soundings there were either large data gaps or bad data at an elevated level, and all of the data above the problem level were removed from the analysis. Finally, in a total of 41 soundings taken in June–September of 1997 and 1998 (the first two winters with the AIR 5A system) temperatures below −90°C were recorded as missing. In these soundings, all data above the level where the temperature first dropped to −90°C were removed. In all, these three quality checks affected about 9% of the soundings and these were distributed fairly evenly throughout all 12 months.

The Dome C data include radiosonde temperatures, fixed 2- and 30-m air temperatures and snow-surface temperature. The air temperatures were measured with YSI 44033 thermistors in ventilated shields. These thermistors have a published accuracy of ±0.1 K, but when the two thermistors were compared side by side at the beginning of the season they agreed to within 0.01 K in an ice bath, and to within 0.03 K outside at −21°C. The surface temperature was measured with a Heitronics KT19.82 infrared thermometer that looked at the snow at an angle of about 45°. The instrument measures the brightness temperature of the snow by looking in the 8–14-μm band. Since the emissivity of the snow is slightly less than 1.0, the actual temperature is about 0.5 K higher than the brightness temperature measured at this angle (Dozier and Warren 1982). Dealing with this small error is preferable to dealing with the potentially much larger radiation-induced errors associated with trying to measure the snow-surface temperature in situ during sunlit times (Brandt and Warren 1993). Radiosonde data at Dome C were collected using Vaisala RS80 and RS90 sondes. Two sondes were launched on most days from mid-December 2003–January 2004. The launches were generally timed to correspond to certain satellite overpasses and were most often performed around 1600 and 2300 local standard time (LST; 0800 and 1500 UTC).

3. The temperature profile at South Pole

a. Temperature and inversion statistics between 2 and 22 m

It is worthwhile to examine the annual temperature cycle, shown in Fig. 2, before looking at seasonal statistics. This figure was made using the 10-yr record of 2-m air temperature (T_2) that is used in the rest of this section. The familiar seasonal cycle over the Antarctic Plateau is apparent, with a short, peaked summer, rapidly changing transition seasons, and a long, coreless winter. This term "coreless winter," from the German *kernlose*, was, according to Wexler (1958), coined by Middendorfs and Hann in the early twentieth century and is used to describe the Antarctic winter, during which the average temperature is nearly constant, with no well-defined core of minimum temperatures. The standard deviation curve shows that the winter temperatures are much more variable than those in summer, because in winter the temperature can be affected by clouds that may be much warmer than the surface, by horizontal advection of air of different temperature, by changing wind speeds that affect the vertical mixing of the inversion layer, and by slight vertical motions due to convergence or divergence of the surface winds that move colder air up or warmer air down (Schwerdtfeger 1977). The contrast of day-to-day variability between winter and summer is illustrated in a 1-yr time series shown by Warren (1996). Given the shape of the mean temperature curve, the seasons will be defined as follows: summer is December and January; autumn is February and March; winter is April–September; spring is October and November (Schwerdtfeger 1970a).

Figure 3 shows a typical temperature sounding for a clear sky in winter. The data above 660 hPa are from a routine RS80 sounding performed by the South Pole Meteorological Office, and those below that level are

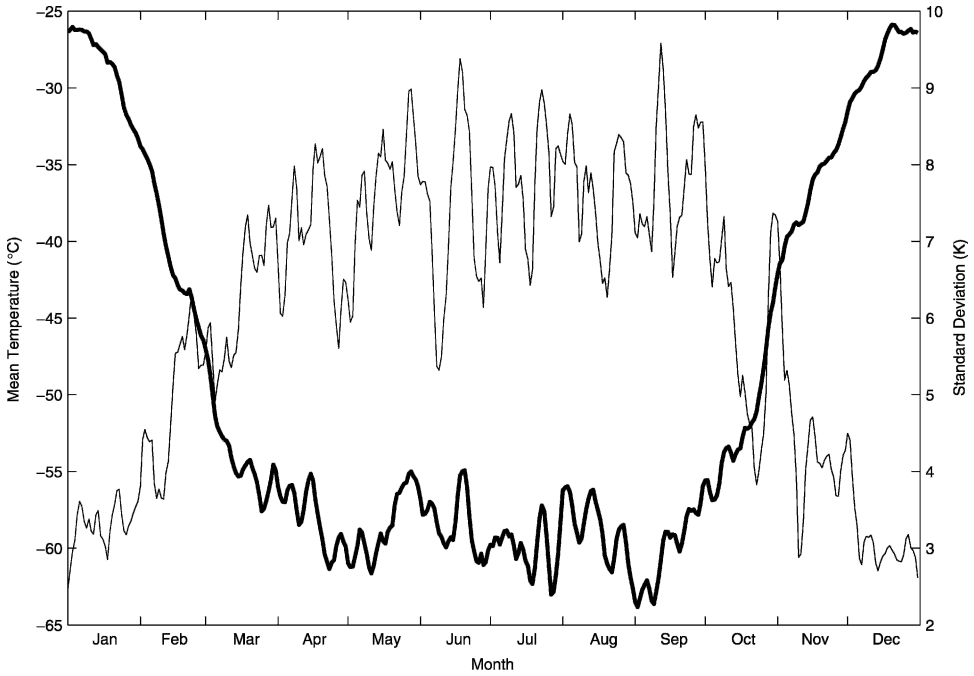

FIG. 2. Mean (thick line) and std dev (thin line) of the 2-m air temperature for each day of the year at South Pole Station (1994–2003). The calculations were done on all the observations of T_2 from the CMDL data for the 5 days centered on each day.

from a tethered RS80 sounding from the South Pole Atmospheric Radiation and Cloud Lidar Experiment (Walden et al. 2001). There is a rapid warming with height very near the surface, with a nearly isothermal layer above that from about 250–900 m. Above that the profile transitions to a more normal lapse of temperature with height. Focusing on Fig. 3b, it is possible to see just how rapid the warming is near the surface. By just 40 m above the surface the temperature is 15 K higher than at the surface, and by 100 m the temperature has risen by 20 K of the total 23-K increase. This concentration of the inversion near the surface is what makes it possible to examine some of its features from a 22-m tower, which in this case would span an increase in temperature of more than 5 K.

The distributions and summary statistics for summer temperatures and inversions are shown in Fig. 4. There are separate distributions for differences between each pair of temperatures: 22 m (T_{22}), 13 m (T_{13}), and T_2. Recall that the data for T_{13} span a much shorter time period than the other data.

From Fig. 4 it is apparent that summer temperatures tend to lie within a fairly small range at all three levels. Over 98% of the T_2 data lie in an 18-K range between −38° and −20°C. Just comparing the T_{22} and T_2 data provides some evidence that there is often an inversion across this layer in summer; every percentile, as well as the maximum and minimum, is lower in the T_2 data, suggesting a tendency for the air to be colder at 2 m than at 22 m. It is also interesting that the difference between these two distributions is larger at low temperatures, where the first percentile is 1.3 K lower for T_2 than T_{22}, than at high temperatures, where the 99th percentile is only 0.3 K lower for T_2. This difference illustrates the fact that the inversion is weaker during warmer periods.

The distribution of the difference between T_{22} and T_2 confirms that, even in summer, inversions occur more than half the time in this near-surface layer. The inversions are often weaker than 1 K over the 20 m, but can sometimes exceed 5 K. Lapses are observed in this layer about 26% of the time. These sometimes exceed the dry-adiabatic lapse rate, but rarely exceed 0.5 K. Interestingly, the 2–13-m layer rarely experiences lapse conditions, while the 13–22-m layer has lapse conditions almost 50% of the time. While inversions are almost always present in the lower layer, the strongest inversions in the lower layer are no stronger than the strongest inversions in the upper layer.

The analogous winter data are presented in Fig. 5. Obviously the temperatures in winter are lower than those in summer, but they are also much more variable, with the middle 98% of T_2 data spanning 34.7 K, nearly twice the value for summer. Also, the effect of the inversion on the T_2 and T_{22} distributions is more apparent

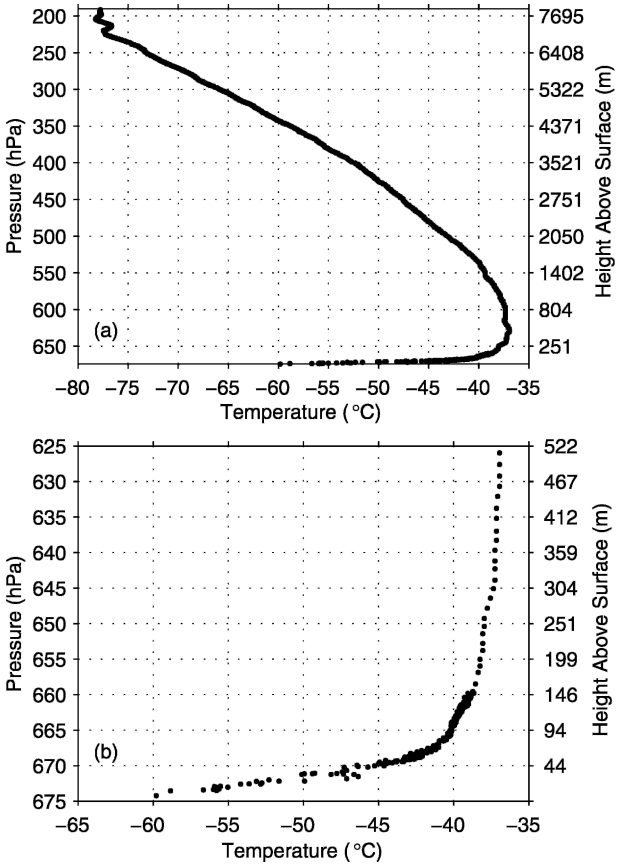

FIG. 3. Temperature profile measured at South Pole Station on 25 Sep 2001. Data above 660 hPa are from a routine radiosounding with an RS80; those below 660 hPa are from a tethered sounding with an RS80. (a) The full tropospheric sounding is shown, and (b) the lowest 500 m are enlarged. The surface pressure was 674 hPa.

in these data; the first percentile of T_2 is 3.3 K lower than that for T_{22}, and the 99th percentile is 1 K lower. The T_2 distribution is seen to be skewed positively, illustrating the ease with which the surface can be warmed in the winter—for instance, by the appearance of a cloud at the top of the inversion—compared to the slower process of cooling radiatively, which requires extended periods of clear skies.

The distributions of temperature differences shown in Fig. 5 show that inversions are more common and can also get much stronger in winter than in summer. Between 2- and 22-m lapse conditions are observed less than 8% of the time, and the median difference is an inversion of 1.7 K. In this 20-m layer inversions sometimes exceed 10 K, and have exceeded 20 K. As in summer, lapse conditions occur much more frequently in the upper layer (13–22 m) than in the lower layer, where they are nearly nonexistent. This difference results in a median inversion strength that is larger in the lower layer than the upper, but the extreme inversions are similar in both layers.

b. *Relationships of T_2 and T_{22} with downward longwave flux and winds*

Using data from CMDL for wind and downwelling longwave flux, this section will show how the temperature and inversion are affected by these two factors. Both are expected to influence the inversion strength and surface temperature. Stronger winds will lead to increased turbulence, mixing warmer air down and decreasing vertical gradients. Increased downward infrared flux, which will occur under clouds or even at times of significant blowing snow (Mahesh et al. 2003; Yamanouchi and Kawaguchi 1984), will cause the surface to warm, or at least reduce its cooling rate. Although the reasons that wind and longwave flux affect the temperature and inversion are easy to see, the resulting relationships are not as simple as might be expected. Only winter data will be shown in this section since that is when the inversion is most pronounced and most variable.

The relationship between T_2 and downward infrared flux is shown in Fig. 6. The dark line shows the median T_2 as a function of downward longwave flux, and the lighter lines show the 10th and 90th percentiles. The most obvious aspect of this plot is that T_2 increases with increasing flux, as expected. There is also a decrease in variability for fluxes below about 80 W m^{-2}. One very interesting feature of Fig. 6 is that T_2 does not seem to increase in the same fashion across the whole range of observed fluxes. The slope of the median curve decreases around 90 W m^{-2}, then begins to increase again by 150 W m^{-2}. This indicates that T_2 is less dependent on downward longwave flux in this middle range of fluxes.

To explore this dependence further, the data were filtered to keep only those observations for which, over the period from 5 h before to 1 h after the time of the observation, the difference between the maximum and minimum observed flux was less than 8% of the mean flux for that time. The idea was to examine only those data that represent near-equilibrium conditions. These filtered data are shown in Fig. 7, as a scatterplot and a line showing the median as a function of infrared flux. Here it is clear that in the filtered data, representing times when conditions were not changing much, there are two preferred regimes in this temperature-flux space. At lower fluxes T_2 is significantly higher than the atmospheric brightness temperature, indicating that the surface is cooling radiatively. At higher fluxes the surface is in radiative equilibrium or warming radiatively. Conditions apparently do not often remain constant at

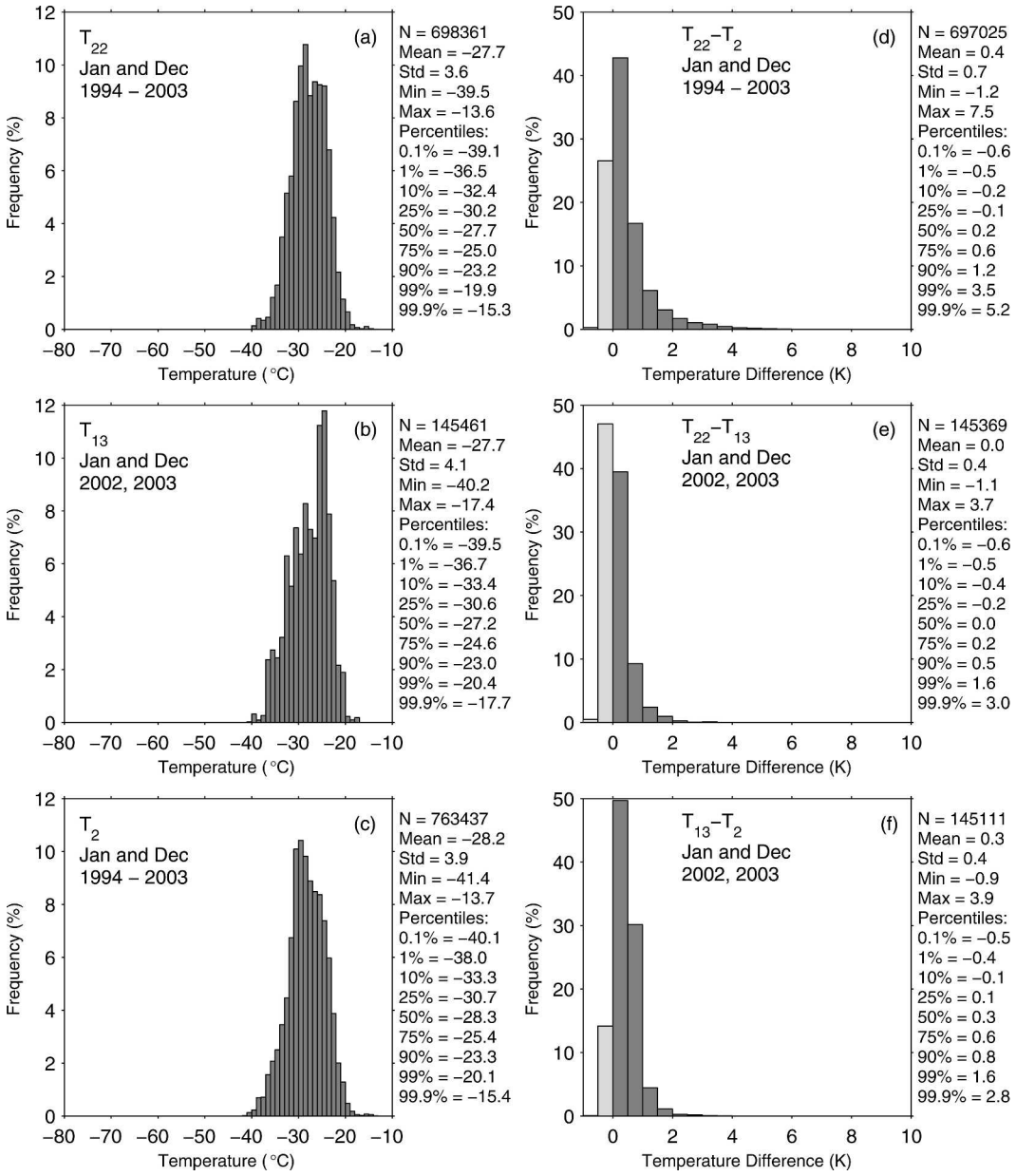

FIG. 4. Distributions and statistics of air temperatures at (a) 22 m (T_{22}), (b) 13 m (T_{13}), and (c) 2 m (T_2), and the differences (d) $T_{22} - T_2$, (e) $T_{22} - T_{13}$, and (f) $T_{13} - T_2$ for summer months. The statistics include the number of observations (N), the mean and std dev (Std) of all observations, the minimum (Min) and maximum (Max) observed values, and various percentiles of the data.

intermediate fluxes, between about 110 and 140 W m^{-2}—that is, in the region with smaller slope in Fig. 6.

A lack of reliable cloud observations in winter made it difficult to better characterize this relationship, which is likely related to clouds. From a preliminary analysis using 3 months of cloud lidar data from winter 2001, it appeared that data in the high-flux region were observed under low clouds; however, many other observations with low clouds fell in the lower-flux group. Perhaps future improved cloud observations, including height and optical depth, will help explain the pattern seen in Fig. 7.

Next, the relationship between winter inversion strength ($T_{22} - T_2$) and downward longwave flux is shown in Fig. 8, using the full dataset. Here again, the obvious feature is what is expected: inversion strength decreases with increasing infrared flux. Also, the variability of inversion strength tends to decrease with in-

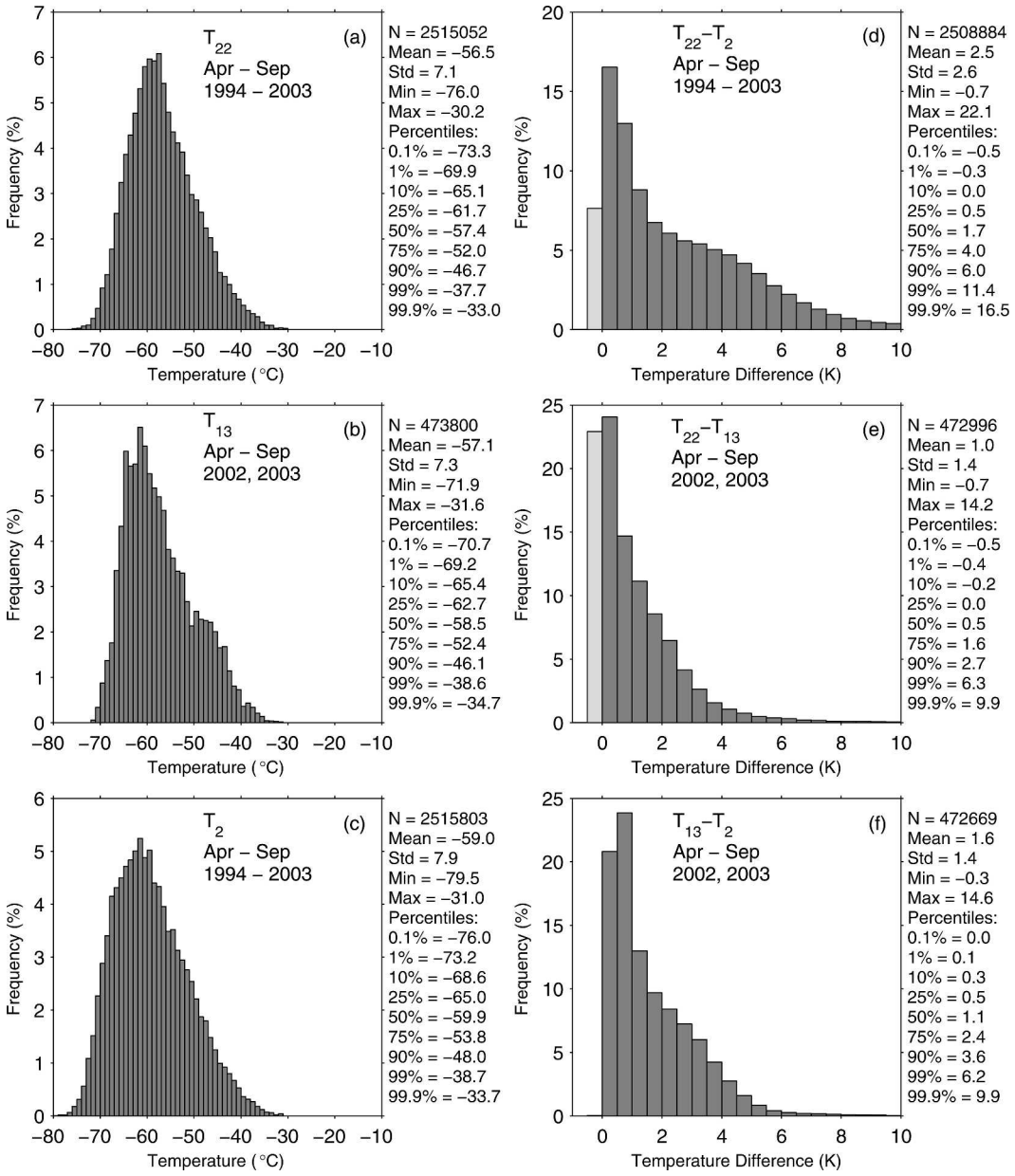

FIG. 5. As in Fig. 4, but for winter months. Note that the abscissas are on fixed scales for comparison (the same scales used in Fig. 4), but the ordinates vary between plots to maximize readability.

creasing flux. The interesting part of Fig. 8 is that the median inversion strength is nearly constant at about 3 K for fluxes less than 80 W m^{-2}, then begins to decrease rapidly, and asymptotes to zero by about 150 W m^{-2}. This decrease begins around 80 W m^{-2}, or an atmospheric brightness temperature of about −79°C, which is near the lowest temperature reached by the surface. This indicates that, as long as the surface is cooling radiatively, the median inversion strength is about 3 K, regardless of the magnitude of the cooling. The difficulty in creating lapse conditions in winter can be seen by the fact that the median asymptotes to zero, rather than dropping below zero for the highest fluxes.

Figure 9 shows how T_2 is related to wind speed. The reason to expect a relationship between temperature and wind speed is that stronger winds will lead to more warm air mixing down from higher in the inversion. The actual relationship does not appear to be so simple. The minimum air temperatures tend to occur with winds of 3–5 m s^{-1}, not with calm winds. A possible cause of the location of this temperature minimum will be presented later in this section.

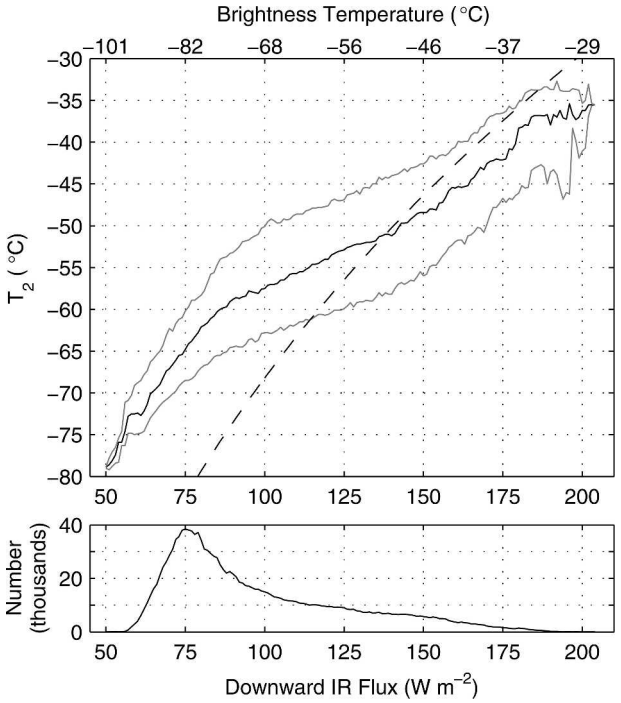

FIG. 6. Median 2-m air temperature (dark line) as a function of downward infrared flux (or corresponding brightness temperature of the sky) in winter; lighter lines are the 10th and 90th percentiles. The dashed curve shows where T_2 would be equal to the brightness temperature of the sky (actual radiative equilibrium between the surface and the sky would occur slightly to the left of this curve because the surface is generally colder than the air at 2 m, and because the surface has an emissivity slightly less than 1). The lower panel shows the number of observations in each bin of width 1 W m^{-2}.

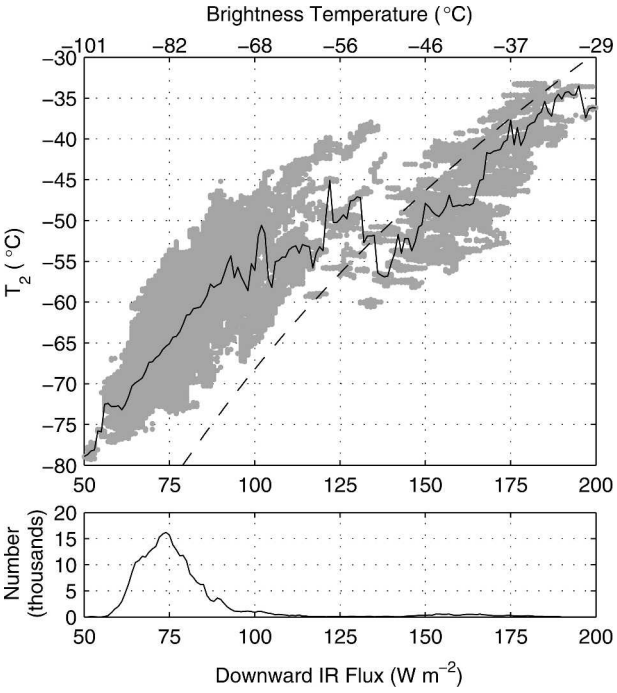

FIG. 7. A scatterplot of filtered, winter T_2 data (gray area) and the median (solid line) of these data as a function of downward infrared flux (or corresponding brightness temperature of the sky). The dashed curve shows where T_2 would be equal to the brightness temperature of the sky. The lower panel shows the number of observations in each bin of width 1 W m^{-2}.

First, let us examine how inversion strength is related to wind speed. Again, the expectation is that stronger inversions can develop with weaker winds because of reduced vertical mixing. Figure 10 shows that this relationship is also more complicated than that. The maximum in the median inversion strength occurs at wind speeds between 3 and 5 m s^{-1}, as did the minimum in temperature. Data from Plateau Station suggest a similar pattern (Riordan 1977), but the 1-yr data record in that paper meant the results were climatologically limited, and Riordan suggested that inversion strength is similar at all wind speeds less than 6 m s^{-1}. These data, with their longer period of record, suggest that this is a real feature of the Antarctic Plateau boundary layer. The 90th percentile curve (i.e., the strength of strong inversions for a given wind speed) has two maxima, one near 3 m s^{-1} and another with very light winds, supporting the idea that very light winds are indeed conducive to the development of strong inversions.

Given that it is unlikely that winds of 3–5 m s^{-1} would promote low temperatures or strong inversions, the causality is probably in the opposite direction. It seems that these relationships could be caused by the "inversion wind," in which the presence of an inversion over gently sloping terrain forces a wind through a local thermal wind. This can be investigated using the model of Mahrt and Schwerdtfeger (1970), who presented a solution for the problem of steady-state flow over uniformly sloping terrain with an exponential temperature profile, assuming a coefficient of eddy diffusivity that is constant with height.

As presented in appendix 4 of Schwerdtfeger (1984), this model specifies the two components of the wind in the boundary layer as functions of height for given conditions as

$$u(z) = (B + v_g)e^{-D}\sin D - (C + u_g)e^{-D}\cos D + Ce^{-z/H} + u_g, \quad (2)$$

$$v(z) = -(B + v_g)e^{-D}\cos D - (C + u_g)e^{-D}\sin D + Be^{-z/H} + v_g, \quad (3)$$

where $u(z)$ and $v(z)$ are the eastward and northward components of the wind at height z, u_g and v_g are the eastward and northward components of the geostrophic

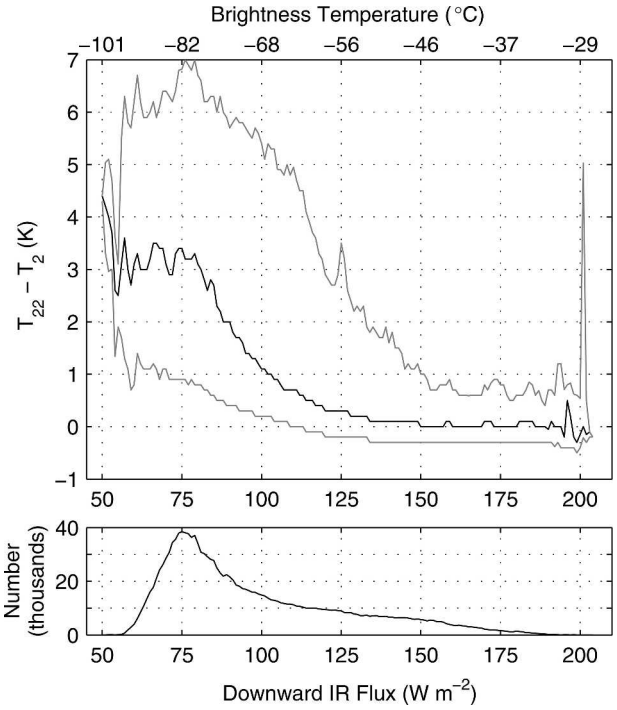

FIG. 8. Median inversion strength (dark line) in the 2- to 22-m layer as a function of downward infrared flux (or corresponding brightness temperature of the sky) in winter; lighter lines are the 10th and 90th percentiles. The lower panel shows the number of observations in each bin of width 1 W m^{-2}.

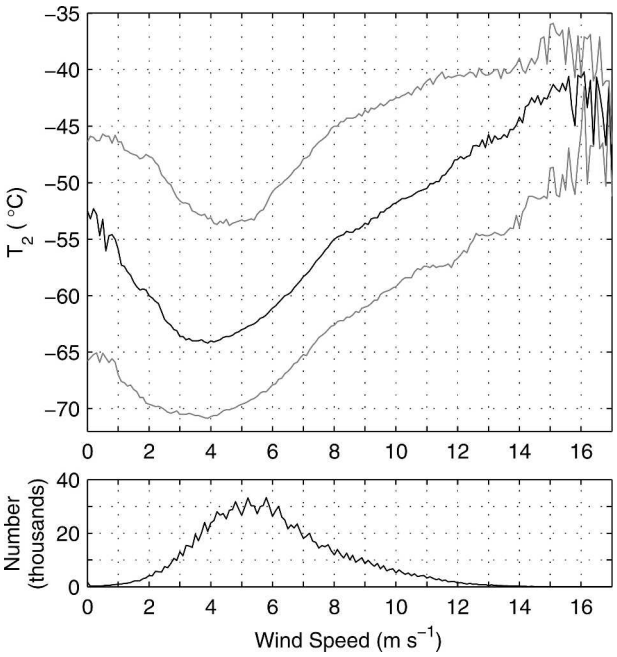

FIG. 9. Median 2-m temperature (dark line) as a function of wind speed in winter; lighter lines are the 10th and 90th percentiles. The lower panel shows the number of observations in each bin of width 0.1 m s^{-1}.

wind at the top of the inversion, H is the e-folding depth of the inversion (50 m in the example given in the next paragraph), and

$$B = -\frac{H^4 f^2 v_T + H^2 |f| K u_T}{K^2 + H^4 f^2}, \quad (4)$$

$$C = \frac{H^2 |f| K v_T - H^4 f^2 u_T}{K^2 + H^4 f^2}, \quad (5)$$

$$D = \left(\frac{|f|}{2K} z\right)^{0.5}, \quad (6)$$

in which f is the Coriolis parameter, K is the coefficient of eddy diffusivity, and $u_T = (g/f)(\Delta T/T)(\partial h/\partial y)$ and $v_T = (-g/f)(\Delta T/T)(\partial h/\partial x)$ are the thermal wind components at the surface, in which g is the acceleration due to gravity, ΔT is the total inversion strength, T is the temperature at the top of the inversion, and $(\partial h/\partial x)$ and $(\partial h/\partial y)$ are the components of the slope in the eastward and northward directions.

Using this model we can test whether the inversion alone at South Pole can create a wind of about 4 m s^{-1}. To do this the temperature profile was assumed to be $T(z) = 235–25e^{-z/50}$, where z is the height above the surface in meters, and $T(z)$ is the temperature in Kelvin at z. This gives a surface temperature of −63°C, and a temperature at the top of the inversion of −38°C. To isolate the effect of the inversion on the wind, it was assumed that there was no large-scale pressure gradient (the geostrophic wind at the top of the inversion was zero). The surface slope was set to 2.25×10^{-3}, with a fall line directed toward 285°. This slope was the average slope over the area from 20 km west to 80 km east of the pole, and from 20 km south to 80 km north of the pole [all directions around South Pole are given on the local grid, where "north" (000°) is parallel to the Greenwich meridian in the direction of Greenwich], as determined from a 1-km-resolution digital elevation model (Liu et al. 2001). This area was chosen to emphasize the slope in the area that is usually upwind of South Pole. The final parameter for the model, the eddy diffusivity coefficient, K, is not well known, so results with two values are compared. Assuming an eddy diffusivity of $K = 0.1$ m^2 s^{-1}, the value assumed by Mahrt and Schwerdtfeger (1970), we get a 10-m wind of 3.4 m s^{-1} from 067°. From estimates made using Monin–Obukhov similarity theory (Garratt 1992) it seemed that a value close to 0.05 m^2 s^{-1} might be more appropriate for these conditions, in which case the resulting wind at 10 m is 5.0 m s^{-1} from 061°. Both results support the idea that the inversion wind can explain the

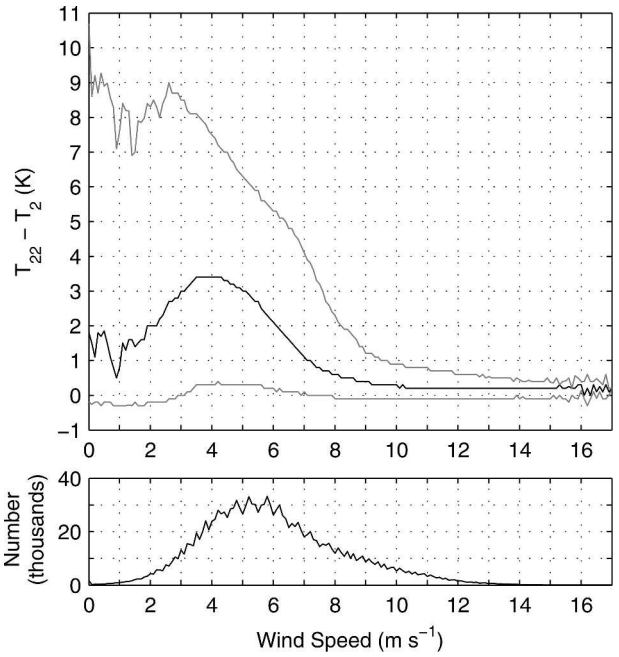

FIG. 10. Median inversion strength (dark line) in the 2- to 22-m layer as a function of wind speed in winter; lighter lines are the 10th and 90th percentiles. The lower panel shows the number of observations in each bin of width 0.1 m s^{-1}.

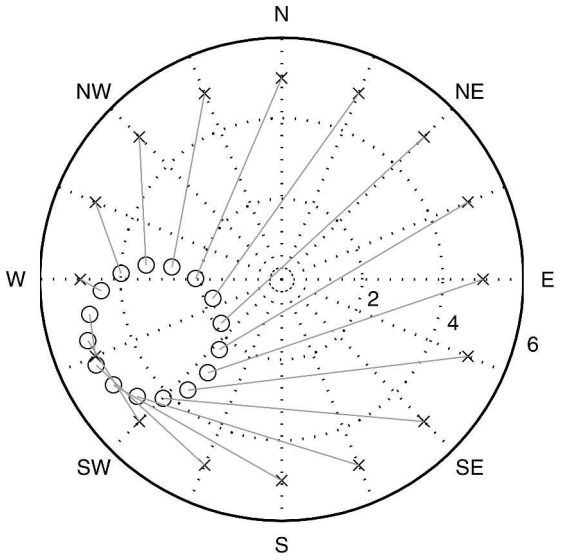

FIG. 11. Winds generated by the inversion under various synoptic conditions. The crosses indicate end points of geostrophic wind vectors at the top of the inversion. Each is connected by a line to a circle that indicates the end point of the resulting 10-m wind calculated with the inversion wind model using the corresponding geostrophic wind to specify the synoptic pressure gradient. For example, with a geostrophic wind at the top of the inversion of 5 m s^{-1} from the south (indicated by the cross at the top of the plot), the inversion wind model predicts a 10-m wind of just over 2 m s^{-1} from the east (indicated by the circle that is attached to the cross at the top). Radial grids are at 2 and 4 m s^{-1}. The downslope direction is 285°.

location of the maximum in inversion strength and the minimum in T_2.

In essence, while the development and maintenance of a strong inversion is favored by light winds, the existence of the inversion can create a wind. This suggests that near the tops of the domes of the plateau, where the surface slope is approximately zero and an inversion therefore cannot create a wind, stronger inversions may be possible under weak synoptic pressure gradients.

Figure 11 shows that this inversion wind model also can explain why winds near the surface at South Pole blow almost exclusively from the northeast quadrant. This figure shows that, for the conditions given in the previous paragraph and an eddy diffusivity coefficient of 0.1 m^2 s^{-1}, a geostrophic wind of 5 m s^{-1} from any direction at the top of the inversion results in 10-m winds that come from grid directions between 038° and 096°. While Neff (1999) clearly shows that this inversion wind is not the only factor driving the winds at South Pole, it does seem that the inversion will often help to ensure that winds will blow from the northeast quadrant under a variety of synoptic-scale influences.

Finally, it is interesting to examine the relationships that exist between these observations and wind direction. Table 1 shows the annual and seasonal vector-mean winds, along with those for very warm and cold periods, and times with very strong inversions. Overall, the resultant wind is from the northeast, at about 4 m s^{-1}, weaker in the summer and stronger in the winter. There is a tendency for spring and summer winds to have more of a northerly component compared to those in autumn and winter.

Winds at times of the strongest inversions have more

TABLE 1. Vector mean winds and directional constancy (vector mean wind speed divided by scalar mean wind speed) at South Pole for various subsets of the data.

	Speed (m s^{-1})	Direction (°)	Constancy
All data	4.2	40	0.75
Summer	3.0	30	0.69
Autumn	4.1	46	0.77
Winter	4.6	43	0.76
Spring	4.4	27	0.76
Winter:			
$T_{22} - T_2 > 15$ K	3.2	76	0.86
$T_2 < -75$°C	3.8	87	0.92
$T_2 > -35$°C	7.0	349	0.78
Summer:			
$T_2 < -38$°C	3.0	92	0.94
$T_2 > -18$°C	8.9	358	0.92

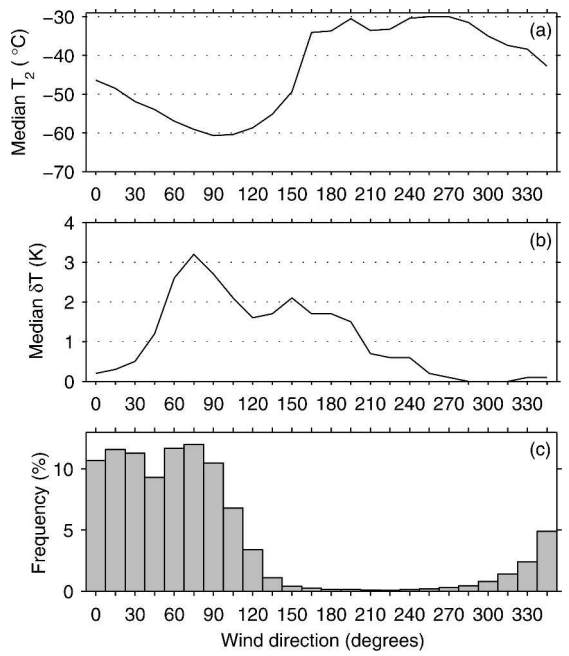

FIG. 12. (a) The median 2-m air temperature and (b) median inversion strength between 2 and 22 m as functions of wind direction. The frequency of winds from each direction is shown in (c). Data are for the entire year and were grouped into 15° bins centered on 000°, 015°, . . . , 345°.

of an easterly component, and are slightly weaker than the overall average. In both summer and winter the lowest temperatures occur with winds from the east, while the highest occur with winds from the north to north-northwest, as pointed out by Hogan et al. (1979).

Another way to consider this relationship between temperature and wind direction is to look at the median temperature and inversion strength as a function of wind direction, shown in Fig. 12, for the entire year. This figure shows the predominance of winds from the northeast quadrant discussed above. Here we again see that the lowest temperatures occur with winds out of the east, which are winds blowing down slope from the higher, colder parts of the plateau. However, in contrast to the resultant winds in Table 1, we now see the highest temperatures occurring with winds from the west, and that winds from the south through the northwest are usually accompanied by very high temperatures, but are also extremely rare.

c. Inversion statistics between the surface and 2 m

Data from a string of thermistors maintained at South Pole in the winter of 2001 are presented here to extend the description of the inversion to the lowest layer of the atmosphere, between the surface and 2 m above the surface.

The height of the thermistors was adjusted approximately every 3 days to ensure the lowest thermistor was right at the surface. In the time between adjustments drifting or falling snow sometimes buried the surface thermistor, and drifting occasionally caused it to be slightly above the surface. Since the temporal variability of temperature below the snow surface is less than that in the near-surface air, we determine whether the surface thermistor is buried by comparing the standard deviation of its time series with that of the 0.2-m thermistor. If, for the 5-h period centered on an observation, the standard deviation of the temperature measured by the surface thermistor exceeded the standard deviation of the temperature measured by the 0.2-m thermistor and all of the data are available from that 5-h period then the surface thermistor is assumed to be at or above the surface, and the observation is used in this analysis. It was unusual for the surface thermistor to be above the surface, and when it did happen it was usually within 0.05 m, so no attempt was made to remove these observations.

Additional quality control of the data included removing observations in which the temperature difference between the surface and 2 m differed in sign from the difference between 0.2 and 2 m, and removing observations in which the temperature difference between the surface and 2 m showed an inversion of more than 4 K or a lapse of more than 1 K. Inspection of the few periods outside of this range indicated that those data were likely in error. These two criteria each resulted in the removal of 2.5% of the data.

Figure 13 shows the median difference between the

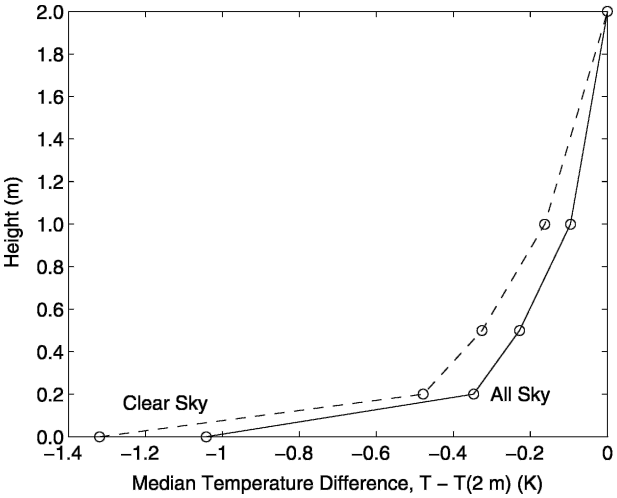

FIG. 13. Median temperature difference relative to 2 m. Data are from South Pole during the 2001 polar night. Separate profiles are shown for the overall median (All Sky, solid line) and the clear-sky median (dashed line).

temperature at each height and that at 2 m, for the sunless period, 21 March–21 September 2001. Two median profiles are shown: the solid line is for all-sky conditions; the dashed line is for times with clear skies. Downward infrared flux data from an upward-looking pyrgeometer were used to determine when skies were clear, using the method described by Town et al. (2005), which determines a clear-sky threshold for each month by modeling the downward infrared flux from a clear sky with the Line-By-Line Radiative Transfer Model using the average atmospheric conditions for that month.

It turned out that the subset of data that included only those observations when the surface thermistor was not buried oversampled nonclear skies. To correct for this, the all-sky data shown in this section include all of the clear-sky data when the surface thermistor was not buried and a random sample of the non-clear-sky data when the surface thermistor was not buried. The size of the random sample was chosen so that the fraction of clear-sky data was 50%, which is what it was in the full dataset, including times when the surface thermistor was buried.

As expected, Fig. 13 shows that the median temperature differences under clear skies were considerably larger than those for data including all-sky conditions. At the surface, temperatures were slightly more than 1.0 K lower than at 2 m in the all-sky median, and were about 1.3 K lower in the clear-sky median. The largest temperature gradient occurs in the lowest layer, so that the median temperature difference between 0.2 m and the surface exceeds 0.8 K under clear skies. Above this layer the gradient weakens, but under clear skies it is still more than 0.25 K m^{-1} between 0.2 and 2 m.

Histograms of the temperature difference between 2 m and the surface are shown in Fig. 14 to give a sense of the variability observed. Figure 14a includes all-sky conditions, while Fig. 14b includes only the clear-sky observations. In both cases the temperature difference is most often between 0 and 2 K. Some lapses were observed in this layer, but never under clear skies.

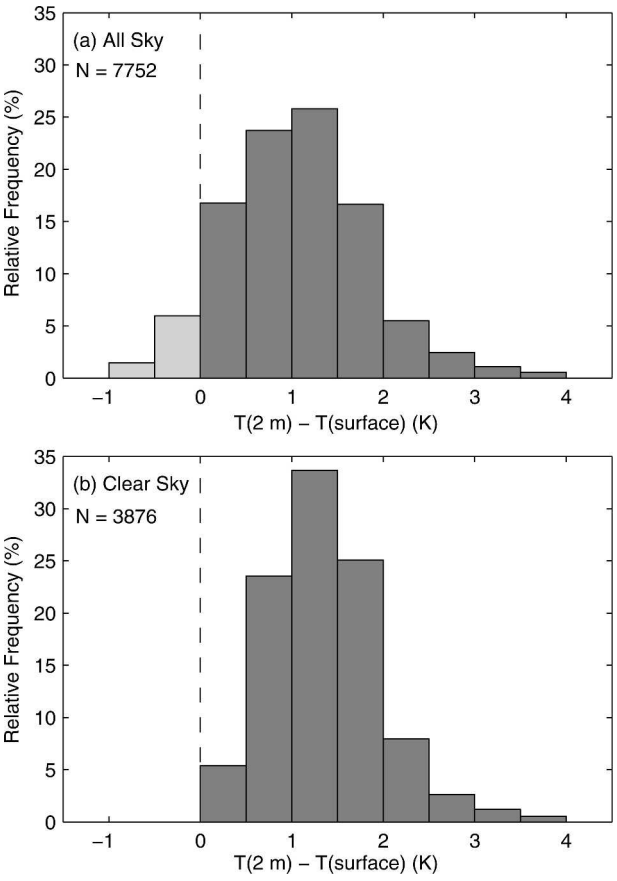

FIG. 14. Relative frequencies of observed temperature differences between 2 m and the surface during the 2001 polar night. (a) The data from all-sky conditions and (b) those from clear-sky conditions.

d. The tropospheric and lower-stratospheric temperature profile

Radiosonde data from South Pole from 1994–2003 were used to create monthly mean temperature profiles from the surface to 30 km above mean sea level (MSL). For the lowest 55 m (2835–2890 m MSL) data from the tower rather than the sonde were used to avoid erroneously warm readings resulting from the preparation of the sondes inside a heated building (Mahesh et al. 1997). This height was usually reached about 10 s after launch, which is approximately twice the *e*-folding response time of the temperature sensors (Hudson et al. 2004), eliminating most of the effect of the heated building. The 2- and 22-m temperatures from the tower at the time of launch were inserted into the lowest part of each sounding and a linear interpolation was made from the tower temperature at 22 m to the radiosonde temperature at 55 m. To correct for the response time of the temperature sensor on the radiosondes, the measured temperatures were shifted back in time by 6 s, assigning each temperature measurement to the height of the sonde 6 s earlier. Mahesh et al. (1997) found that this method was as effective at correcting profiles as a more complicated deconvolution method. The data from each sounding were then linearly interpolated to a fixed set of heights: every 10 m from 2890 to 3000 m MSL, every 20 m from 3020 to 3500 m MSL, every 50 m from 3550 to 4500 m MSL, and every 100 m from 4600 to 30 000 m MSL. Then every interpolated sounding from each month was used to produce the plots in Figs. 15–17. In these monthly mean profiles the effect of the

response time correction is largest in the middle of the inversion layer, where it can increase mean temperatures by 2 K in winter months (since the reported temperature is still influenced by the much colder air just below the sonde's position); above the inversion its effect was generally less than 0.25 K.

Each of these plots shows the monthly mean air temperature as a function of height as a solid line; they also include dashed lines showing the 10th and 90th percentiles of air temperature as a function of height. Three profiles are presented for each month. All show the same data, but the latter two show successively more detail in the lower atmosphere.

Figure 15 shows the soundings from the surface to 30 km MSL. In these we can focus on the progression of the temperature in the upper troposphere and lower stratosphere. During January and February the temperature profiles resemble those at lower latitudes, with a well-defined tropopause around 8–9 km and significant warming in the stratosphere. As the sun sets in March the stratosphere begins to cool, rapidly above about 15 km, so that by May the area between 15 and 30 km is colder than any part of the troposphere. The lower stratosphere does not cool as quickly, so a tropopause is still apparent in May, and, to some extent, in June.

Before looking at the rest of the year it is worth mentioning that in winter very few of the balloons make it through the extremely cold air in the stratosphere. As a result, the winter profiles above about 10–15 km are based on relatively few observations.

Moving on, by July and August there is virtually no sign of a temperature tropopause and the air around 20 km has cooled to about $-90°$C, a temperature not reached in the troposphere or stratosphere anywhere outside Antarctica, and which permits the formation of polar stratospheric clouds and enhances ozone depletion (Solomon 1990). By August and September the highest parts of these soundings are seeing the sun and begin to warm. The warming continues throughout October and November, when temperatures at 30 km are higher than in any part of the troposphere in any month. However, a temperature tropopause is not clearly reformed until December. Comparing December and January we see that the lower stratosphere continues to warm, while the upper parts of these soundings are already cooling.

It is necessary to explain the unusual features seen in the September profile in Fig. 15. From all of the September data only 98 of the 314 soundings continue above 15 km. Of those, eight were from late September 2002. In that year the stratosphere warmed unusually early, so that temperatures in those eight soundings from about 10–15 km and up were much higher than in any other September sounding. Between the 0000 UTC soundings on 20 and 23 September the temperature rose by about 4 K at 10 km, by about 15 K at 15 km, and by almost 42 K at 21.5 km. The presence of these eight warm soundings raises the mean enough so it is greater than the 90th percentile in places. Six of these eight soundings continued above 30 km, and the other two reached 28 km, while the total number of soundings available had dropped to 73 by 22 km. By that point, the 90th percentile jumps to the warm group of soundings, which explains the discontinuity in that line. The fact that soundings are more likely to reach higher levels at times of higher temperatures indicates that mean profiles could be biased warm at these heights whenever there is a lot of variability in temperature.

Figure 16 shows the profiles from the surface to 10 km MSL. These also show the loss of the temperature tropopause between April and June. It is also apparent that the temperature structure in the free troposphere does not vary much during the year. The mean temperature at 6 km varies by less than 12 K during the year, and by only about 3 K during the winter (April–September).

The temperature structure of the lowest kilometer of the atmosphere is shown in Fig. 17. This shows the details of the full inversion, as well as some of the isothermal layer above the inversion. The profiles for the two summer months show only a very slight, shallow inversion, with nearly isothermal conditions in the lowest kilometer. In February a significant inversion is present, as the 2-m temperature drops below $-40°$C. The near-surface temperature continues cooling in March, but then remains nearly constant during the coreless winter; the 2-m temperature drops by just 1.3 K between April and September. In October and November the inversion weakens dramatically as the air near the surface warms much more than the air above it.

The top of the inversion occurs around 600 m in these mean profiles except in summer, when it is closer to 300 m. Temperatures at the top of the inversion drop by less than 2 K between April and August, despite average winter radiational-cooling rates at this height measured to be about 4 K day^{-1} (Schwerdtfeger 1970b). Schwerdtfeger attributed this great reduction in cooling at the top of the inversion to subsidence and, to a lesser extent, warm-air advection.

Table 2 shows the monthly mean temperature gradient between 2 and 100 m, and inversion strength and depth calculated from these mean profiles. The average inversion strength calculated from the individual soundings is also shown, and is 0.5–1 K larger than the inversion in the monthly mean profile because of the

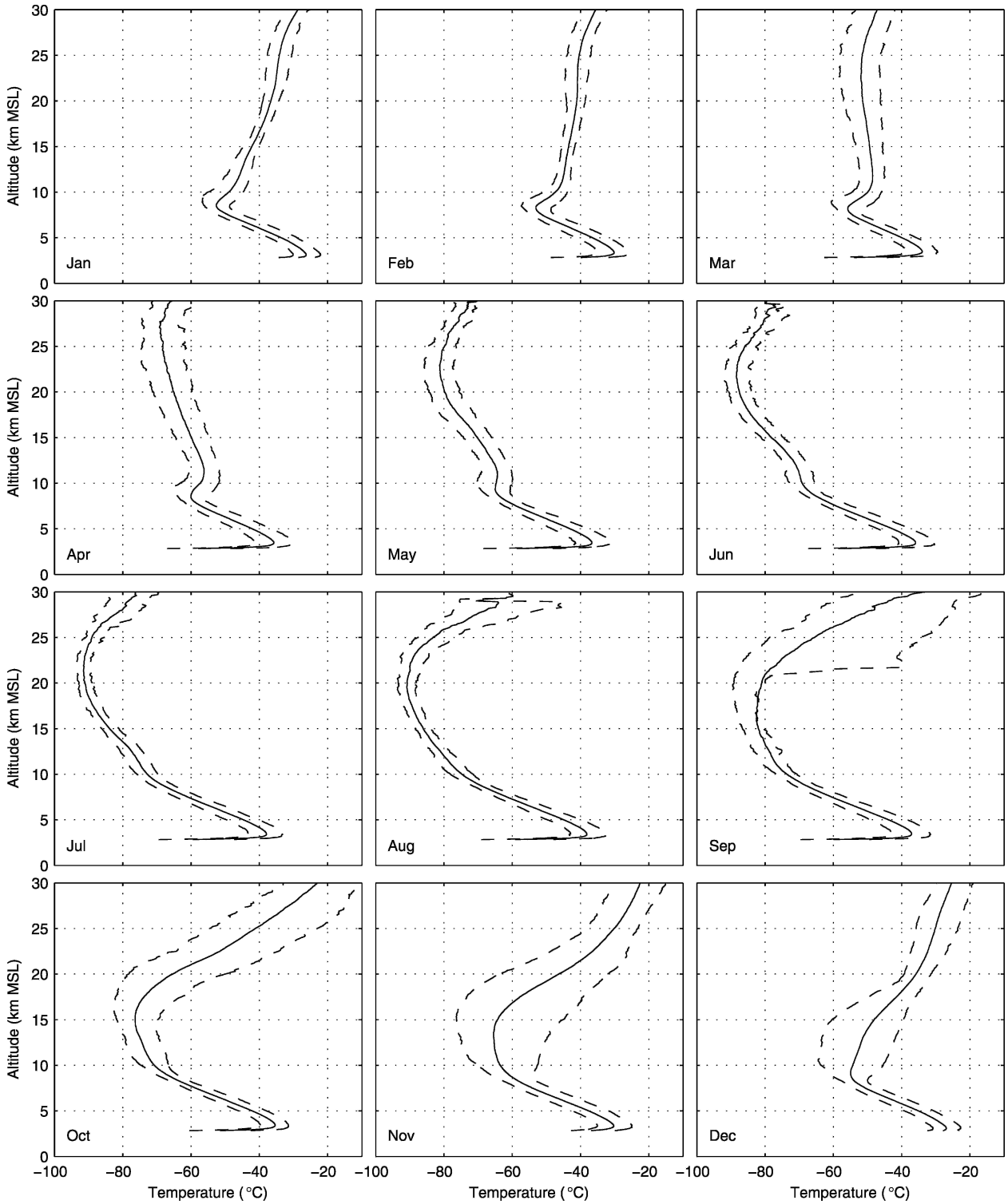

FIG. 15. The monthly mean (solid line) atmospheric temperature profiles from 2 m above the surface to 30 km MSL over South Pole. The dashed lines show the 10th and 90th percentiles of temperature at each height. Radiosonde data begin 55 m above the surface (2890 m), and temperatures from a tower are used at 2 and 22 m. Data from 1994 to 2003 were used.

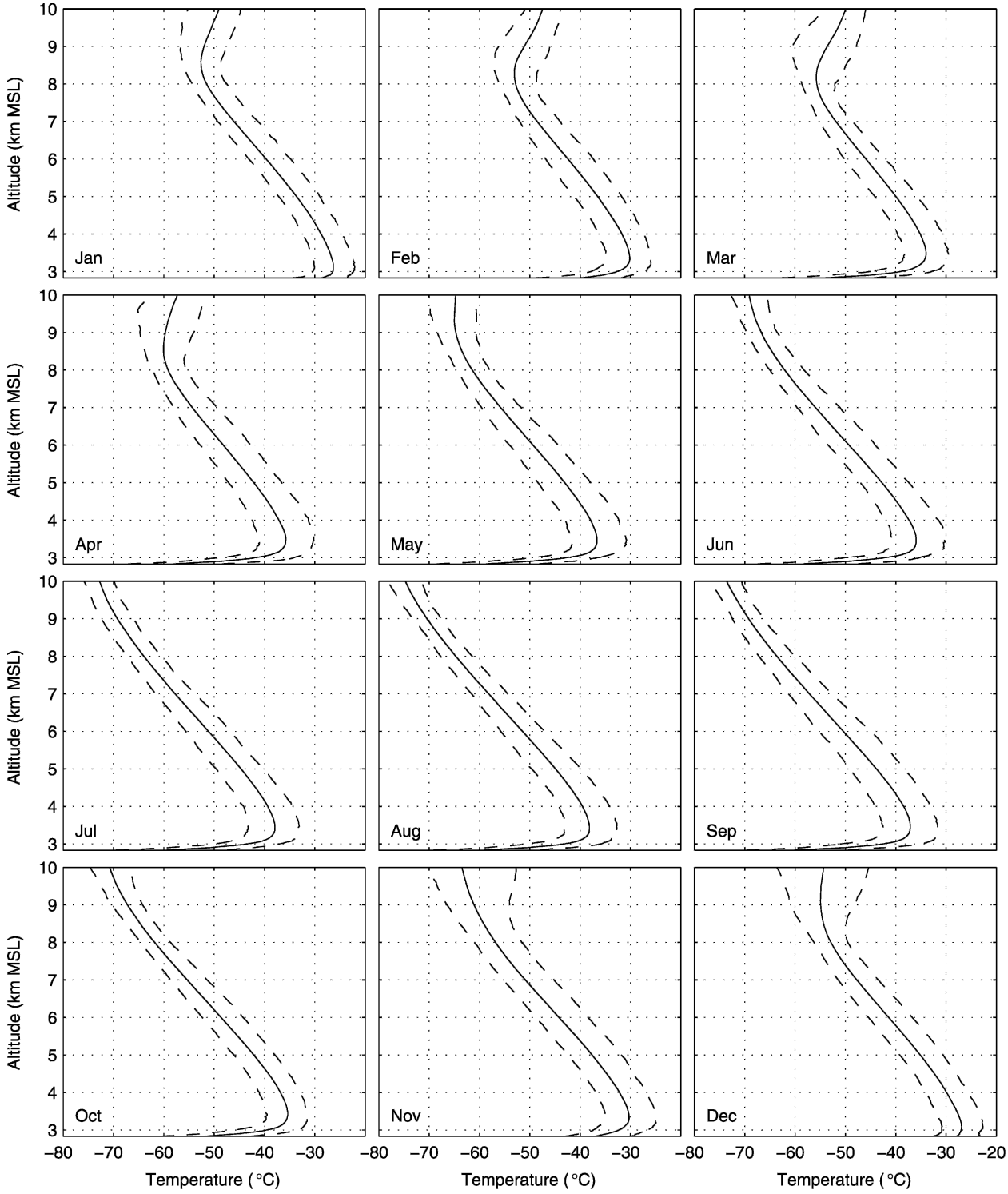

FIG. 16. Same as Fig. 15, but only the lowest 10 km.

variability in the height of the top of the inversion. The fact that the difference between these two inversion strengths is small suggests that the shape of the inversion is very stable. The strength and persistence of the winter inversion is clear; on average, the temperature at 100 m is about 12.5 K higher than at 2 m in September. The last two columns in Table 2 show the values of inversion strength and depth calculated by Dalrymple

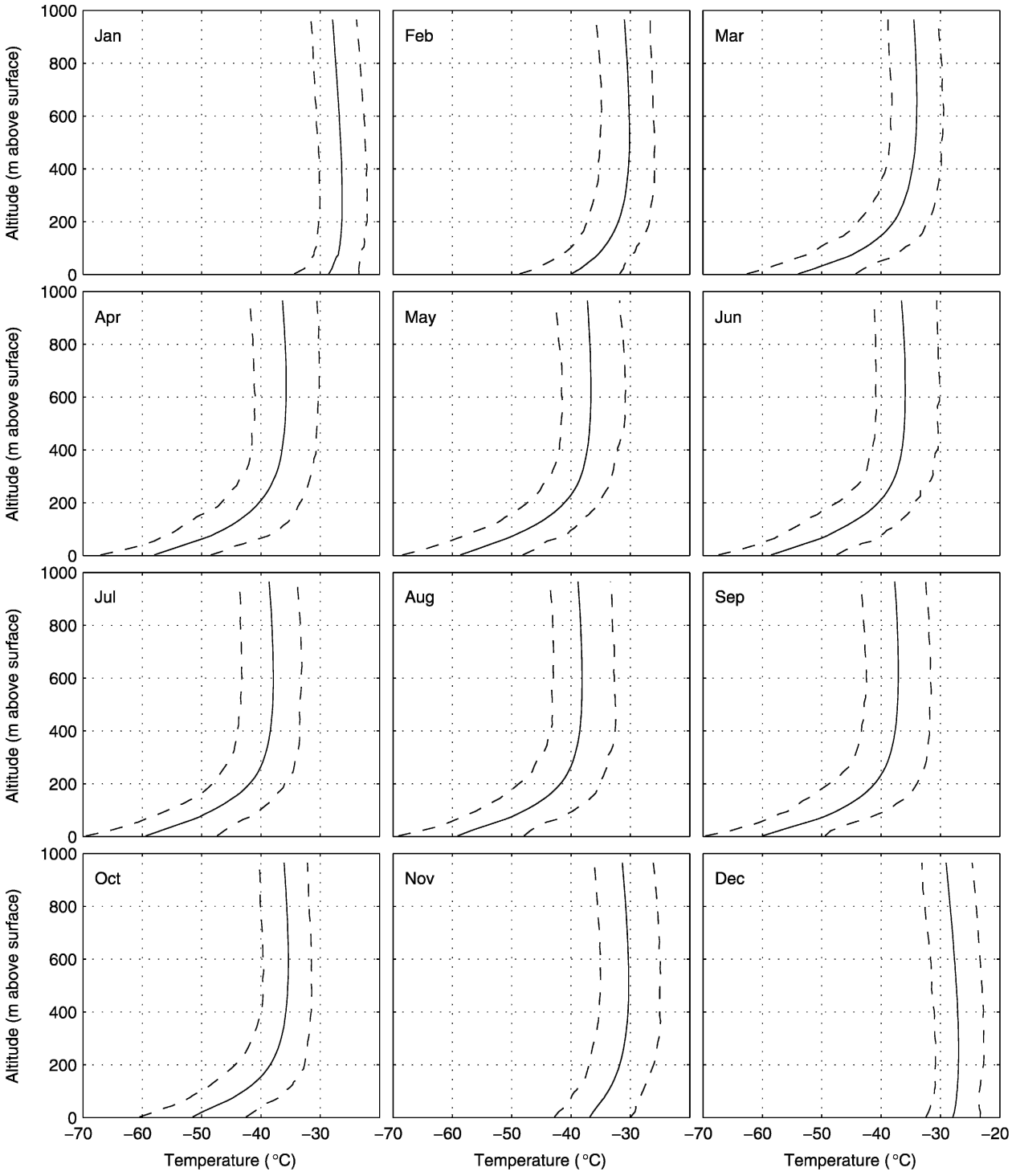

FIG. 17. Same as Fig. 15, but only the lowest 1 km above the surface.

(1966) from individual soundings from South Pole from November 1958–October 1961. These values suggest that there has been no large change in the inversion structure at South Pole during the last four decades. The consistently higher height of the top of the inversion reported by Dalrymple is more likely to be due to improvements in radiosonde response time than to real changes in the inversion structure.

TABLE 2. Monthly mean temperature gradient between 2 and 100 m above the surface ($\partial T/\partial z$), inversion strength between 2 m and the warmest point in the troposphere calculated from the monthly mean sounding (ΔT_{mean}) and from each individual sounding (ΔT_{sound}), inversion depth (ΔZ) calculated from the monthly mean sounding. All of these values were determined from 10 yr of data. Also shown for comparison are the values presented in Dalrymple (1966, his Table 30) for data from Nov 1958 to Oct 1961 (ΔT_{Dal} and ΔZ_{Dal}).

Month	$(\partial T/\partial z)$ (K m^{-1})	ΔT_{mean} (K)	ΔT_{sound} (K)	ΔZ (m)	ΔT_{Dal} (K)	ΔZ_{Dal} (m)
Jan	0.018	2.3	3.1	265	3.4	357
Feb	0.054	9.8	10.6	525	10.6	609
Mar	0.111	20.0	20.7	665	20.0	685
Apr	0.118	22.2	22.8	665	23.5	706
May	0.113	22.0	22.6	605	21.1	657
Jun	0.116	22.6	23.3	625	21.8	644
Jul	0.113	21.5	22.1	585	20.0	641
Aug	0.114	21.0	21.6	605	22.0	638
Sep	0.128	22.9	23.6	605	20.5	669
Oct	0.085	16.1	16.8	585	15.5	596
Nov	0.030	6.6	7.3	505	7.7	546
Dec	0.007	1.0	2.0	245	2.3	319

It is interesting to compare these results with the Arctic. Looking at monthly mean soundings from Barrow, Alaska, and Eureka, Nunavut, Walden et al. (1996) found that the inversion depth was around 1000 m at these sites in winter, and the strength was about 10–12 K. At Barrow and Barter Island, Alaska Kahl (1990), found similar winter inversion strengths, and median depths between 600 and 900 m by examining the strengths and depths from all individual soundings. Also, Serreze et al. (1992) found that the median inversion depth at the Soviet drifting stations in the Arctic Ocean in winter was around 1200 m, and the median strength was around 12 K. In all these studies the polar-night inversions in the Arctic were found to be much weaker and at least somewhat deeper than what is observed at South Pole.

4. Case study of inversion destruction

The large day-to-day variability of T_2 in winter (Fig. 2) is largely due to the ability of clouds and wind to rapidly destroy the inversion. Here we examine a case study. On 8 September 1992 a very strong inversion was quickly eroded as T_2 increased when a cloud moved overhead. Temperature data from this day are shown in Fig. 18; T_2 and T_{22} are hourly data from CMDL, and T_{11} is the 11-m air temperature measured on a pyrgeometer. The inversion strength ($T_{22} - T_2$) was very large for several hours and peaked at 19 K; this extreme inversion was responsible for some optical phenomena observed visually at that time (S. Warren 2004, personal communication): looming of the horizon, a ducting mirage, and the Novaya Zemlya Solar Mirage (Greenler

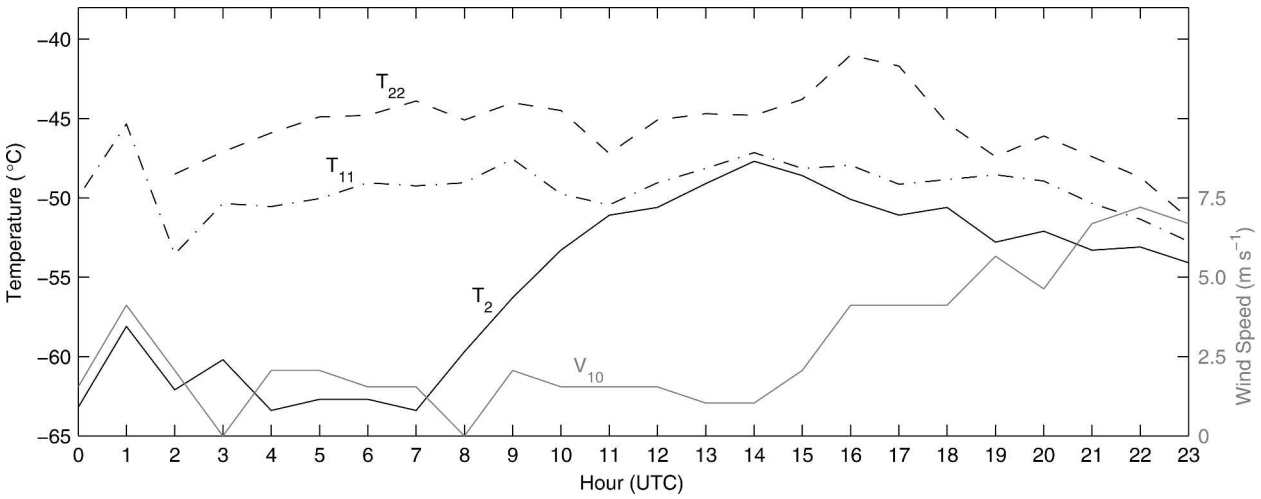

FIG. 18. Air temperatures at 2, 11, and 22 m, and 10-m wind speed (V_{10}) at South Pole on 8 Sep 1992.

1980). In the 7 h after 0700 UTC, T_2 increased by 15.7 K, while the temperature at the two higher levels remained nearly constant. Warren's visual observations indicated that a cloud moved over the station around 0720 UTC, and the measured downwelling longwave radiation increased substantially between 0700 and 0800 UTC. This figure also shows that during the warming the winds were very light, less than 2.1 m s^{-1}, suggesting that they likely played only a small role in the near-surface warming.

Given the light winds and observation of cloud cover, it seems likely that this warming was driven mainly by the increased downwelling longwave radiation. To see if the increase in downwelling radiation could, by itself, cause a temperature increase of this magnitude in this time period, a simple thermal-conductivity model of the snowpack was used to predict the surface temperature. This one-dimensional model included the upper 60 cm of snow, with 1-mm vertical resolution. The temperature change at each layer due to convergence of vertical heat flux was calculated using centered differencing of the following equation:

$$\frac{\partial T}{\partial t} = \frac{k}{\rho c}\frac{\partial^2 T}{\partial z^2}, \tag{7}$$

where T is temperature, t is time, k is the effective thermal conductivity of the snow, $\rho = 345$ kg m^{-3} is the approximate snow density measured at South Pole in 1992 by Brandt and Warren (1997), $c = 2100$ J kg^{-1} K^{-1} is the heat capacity of ice, and z is depth. This equation assumes that k can be taken as constant over a 2-mm layer. An additional term,

$$\frac{\partial T}{\partial t} = \frac{F_d - \varepsilon\sigma T^4}{\rho c \delta z}, \tag{8}$$

was added to the surface temperature change to account for radiational heating and cooling, where $\delta z = 0.001$ m is the thickness of the layer; F_d is the observed downward longwave flux; ε is the snow-surface emissivity, which was set to 1; and σ is the Stefan–Boltzmann constant.

The profile of thermal conductivity was taken from Brandt and Warren (1997), and their snow temperature data for this day at depths of 20, 30, 40, and 60 cm were used to determine the initial temperature profile. The initial surface temperature was assumed to be 3 K lower than T_2 at that time to account for the continuation of the inversion to the surface; while this is a reasonable value for a strong inversion according to the thermistor data presented in section 3c, the actual value of this difference is unknown; however, varying this value by a factor of 2 in either direction has negligible impact on the results of the model. The temperature at a depth of 60 cm was held constant (the measured change during the 11 h simulated was only 0.1 K). The model was initialized at 0400 UTC, and was run, with 0.25-s time steps, until 1500 UTC.

The results of this model are shown as the solid black line in Fig. 19, along with the downward longwave flux used to force the model, and the measured T_2. Unfortunately, there are no measurements of snow-surface temperature for this time, so we can only compare the calculated surface temperature with the measured 2-m air temperature. This simple model indicates that such a warming as was observed can be accounted for by the increased radiation reaching the surface, with no other factors contributing. Adding a sensible heat flux, calculated with Monin–Obukhov similarity theory (Garratt 1992), reduced the warming slightly, but did not have a large effect on the overall picture produced by the model.

5. Diurnal cycle at a lower-latitude site

The diurnal cycle is absent at the South Pole but is significant elsewhere on the plateau. The inversion was studied during the summers of 2003/04 and 2004/05 at Dome C Station (75°S, 123°E). During these periods the sun was always above the horizon, but its elevation angle ranged from 3° to 38°, and varied by about 30° during the course of each individual day.

Figure 20 shows the half-hourly mean temperatures of the surface, and of the air at 2 and 30 m. The data used to create this figure and Fig. 21 were collected from 22 December 2004 to 31 January 2005. The largest diurnal cycle is observed at the surface, where the diurnal range is about 13 K, but the effect of this cycle is seen at all three levels. At the surface the maximum temperature occurs about 2 h after solar noon, while the 30-m temperature maximum lags the sun by nearly 4 h. For several hours around midday the surface is warmer than the overlying air, but at night an inversion is clearly present. Schwerdtfeger (1970a) showed similar data from Plateau Station for February. In those data the air temperature at 0.25 m varied by about 13 K, while at 32 m it varied by only about 2.5 K. However, unlike at Dome C in January, at Plateau in February the near-surface air temperatures remained 1–2 K lower than the 32-m temperature even at midday

The half-hourly mean inversion strength across the three layers is shown in Fig. 21. Here we see that lapse conditions occur in all three layers around local noon. By just after 1500 LST (UTC+8) the surface cools be-

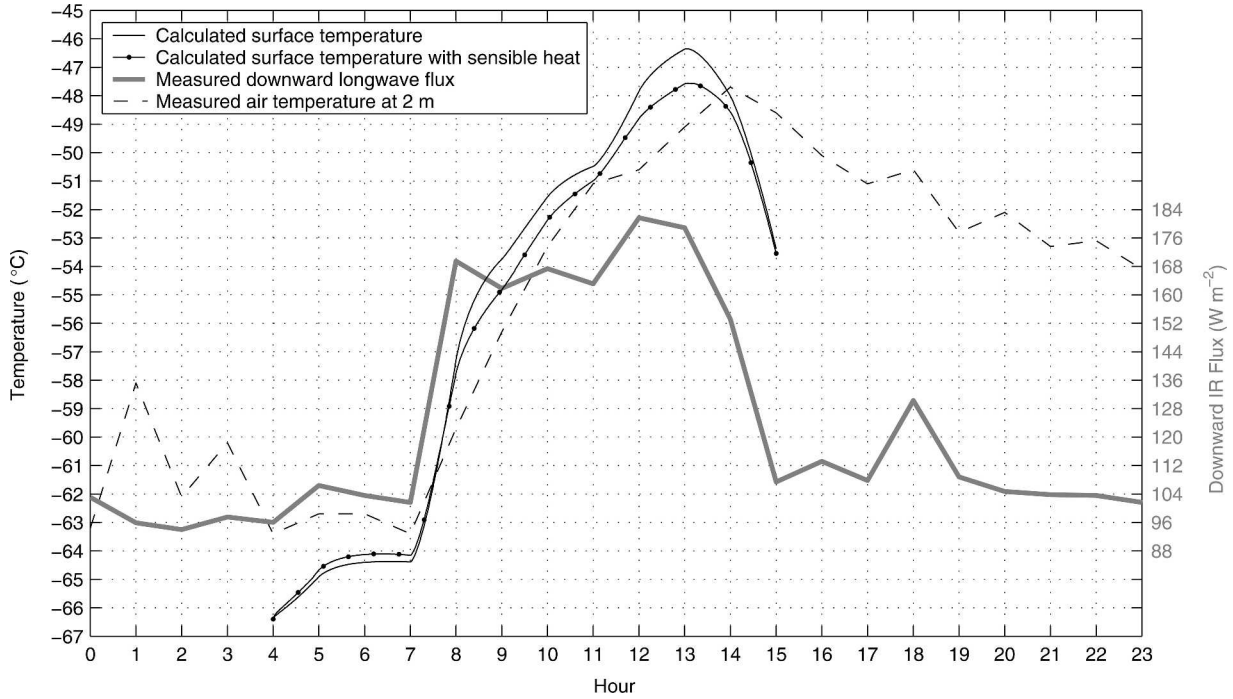

FIG. 19. Results of the snow–temperature model during the warming in Fig. 18 both with and without sensible heat flux. Also shown is the measured T_2 and the downward longwave flux; the latter was used as an input into the model.

low the 2-m air temperature, and around 1700 LST an inversion begins to form between 2 and 30 m. The inversion develops rapidly and, on average, reaches a maximum of 10 K between the surface and 30 m, about 6 K between 2 and 30 m, and about 4 K just between the surface and 2 m. On three nights the inversion in this lowest 2-m layer exceeded 10 K. The layer between 2 and 30 m had inversions exceeding 10 K on about one-third of the nights, with maximum strengths around 13 K. Over the full surface to 30-m layer the inversion strength frequently approached 15 K, but never exceeded 17 K. The mean inversion strength between 2 and 30 m on a summer night at Dome C is stronger than almost any inversion between 2 and 22 m observed at South Pole in summer.

Some radiosonde data from Dome C are presented in

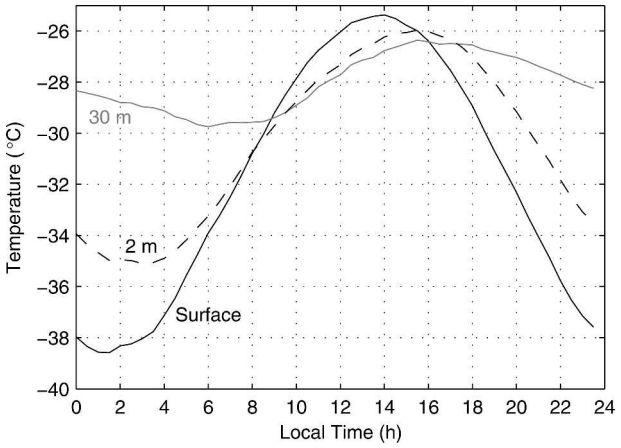

FIG. 20. Half-hourly mean surface temperature and air temperature at 2 and 30 m at Dome C Station for the 2004/05 summer. Time is given in local standard time, UTC+8

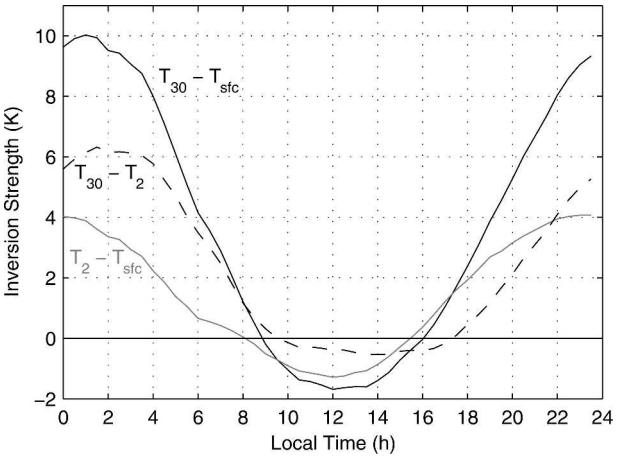

FIG. 21. Half-hourly mean inversion strength across the three available layers at Dome C Station for the 2004/05 summer. Time is given in local standard time, UTC+8

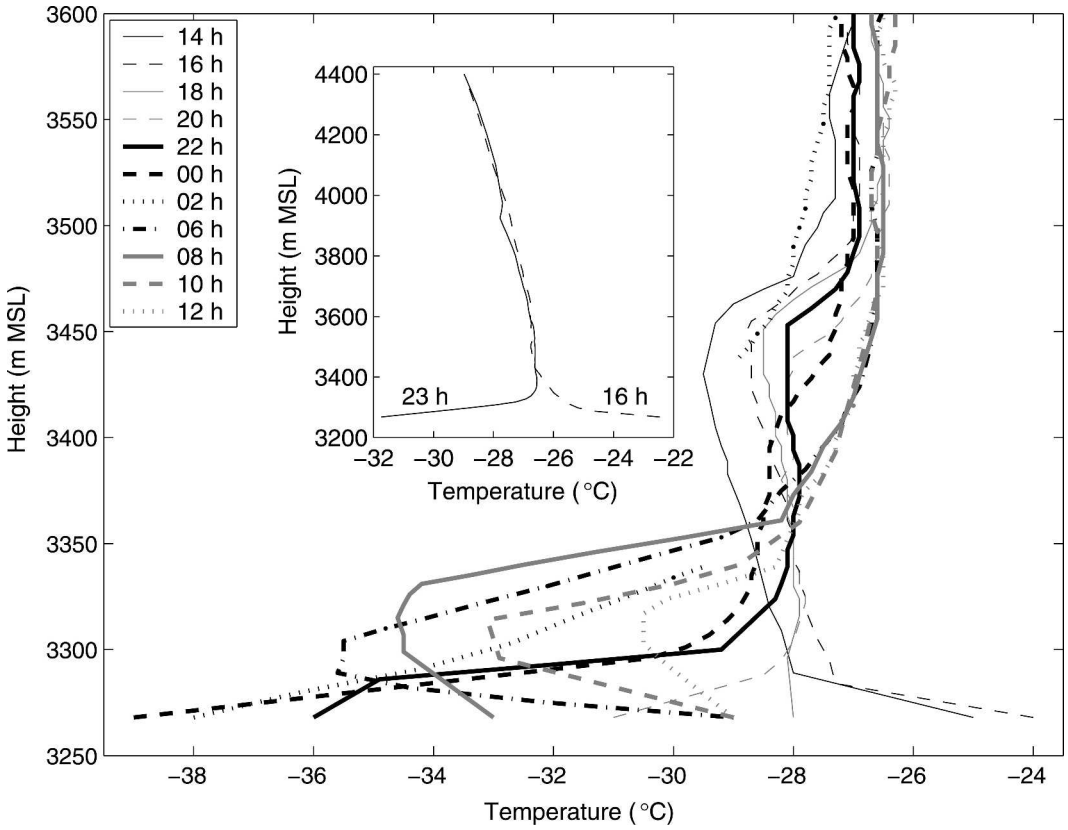

FIG. 22. The main panel shows soundings from Dome C taken every 2 h from 1400 LST 24 Jan 2004 to 1200 LST 25 Jan 2004. The surface is at 3266 m, and the lowest point is the 2-m air temperature measured at the time of launch. The 0400 LST sounding is not available, and the 0200 LST sounding is missing data from approximately 3350 to 3450 m. The inset panel shows the mean temperature profile from all soundings at Dome C taken in the hour centered on 1600 LST (dashed line) and on 2300 LST (solid line). Twenty soundings taken between mid-Dec 2003 and the end of Jan 2004 went into each of these two mean profiles. All times are given in local standard time, UTC+8.

Fig. 22 to show the effect of the diurnal cycle on a deeper layer of the atmosphere. The main panel shows a series of temperature profiles from radiosonde launches every 2 h from the early afternoon of 24 January 2004 through noon on 25 January 2004, presenting one complete diurnal cycle. We see that on this day the maximum near-surface temperature in the 2-hourly data, −24°C, was recorded at 1600 LST, and that the minimum, 15 K lower, occurred 8 h later. Here we can again see the rapid weakening of the diurnal cycle above the surface; by about 100 m above the surface the diurnal cycle is overwhelmed by other forms of hourly variability. Significant lapse conditions are apparent in the first two afternoon soundings, overlain by weaker lapses, with an elevated inversion at about 200 m. By 1800 LST the atmosphere is nearly isothermal up to the elevated inversion. A strong near-surface inversion develops in the lowest 50 m during the evening, but, as the solar elevation angle begins to increase in the early morning hours, the near surface temperature begins to rise. By 0600 LST there is a strong lapse in the lowest 25 m, with the inversion continuing to deepen above that height. The surface warming then ceases, and the elevated temperature minimum weakens through the late morning.

The pattern in the main panel is from one day, and is not meant to represent a mean diurnal cycle, but rather to show the type of effects we may see in the lower atmosphere due to the diurnal cycle. There was unusually dense fog on the night shown here, and that fog dissipated between 0500 and 0800 LST, possibly leading to the cooling seen between 0600 and 0800 LST. This fog may have caused other irregularities in the diurnal cycle on this particular day as well.

The inset panel in Fig. 22 is an attempt to average out the day-to-day variability and show more nearly the average effect of the diurnal cycle. The dashed line is the average of all 20 profiles taken in the hour centered

on 1600 LST from mid-December through the end of January; the solid line is the same, but for those near 2300 LST. These are the two 1-h periods with the most sonde launches. In the mean profiles the effect of the diurnal cycle does not extend more than about 150 m above the surface. This plot shows that the large effect of the diurnal cycle does not extend much above the tower data presented above.

6. Conclusions

The South Pole temperature data from 1994 to 2003 show the usual seasonal cycle of the Antarctic Plateau, with a short, peaked summer and a 6-month, coreless winter. Two-meter air temperatures in summer are usually between −38° and −20°C, while in winter they are much more variable, usually between −73° and −38°C. The lowest temperatures at 22 m are higher than those at 2 m because of the temperature inversion. However, the highest temperatures are similar at both levels because the inversion is generally much weaker on very warm days.

Distributions of temperatures and temperature differences in the 2- to 22-m layer show no surprising results but provide an analysis of conditions in this largely unstudied layer with a period of record at the top and bottom that is long enough to eliminate much of the influence of interannual variability. In summer an inversion is observed between 2 and 22 m nearly 75% of the time, but temperature differences across this layer are usually less than 1 K. Lapse conditions appear to be much more common between 13 and 22 m than between 2 and 13 m, or over the entire layer. The 2- to 22-m layer has isothermal or inversion conditions more than 90% of the time in winter, and these inversions can greatly exceed 10 K. The 13- to 22-m layer in winter is again much more likely to have lapse conditions than the lower layer, although both layers can have equally steep inversions.

Analyses of the variations of temperature and inversion strength with winds and downward longwave flux yielded some surprising and previously unreported results. The 2-m air temperature in winter increases with increasing downward longwave flux, but not uniformly. There seem to be two preferred regimes for these data in near-steady-state conditions, one in which the surface is radiatively warming and one in which it is radiatively cooling. This nonuniform and possibly regime-like relationship has not been discussed before and the physical mechanisms causing it have not been explained. The clear relationship between downward longwave flux and clouds suggests that better cloud observations could help explain this behavior.

The inversion strength does not steadily decrease with increasing flux, but is nearly constant for values of downward longwave flux less than about 80 W m^{-2}, at which time the surface is nearly always radiatively cooling, and then quickly decreases as the flux continues to increase and asymptotes to zero for fluxes greater than 150 W m^{-2}. This is the first long-term study of this relationship and it is interesting to see that the correlation of these two values is limited to the 80–150 W m^{-2} range of fluxes.

The relationships of wintertime temperature and inversion strength with wind speed show some features not previously identified. The minimum temperatures tend to occur not with calm conditions, but with winds of about 3–5 m s^{-1}, as do the strongest median inversions. An analysis of the wind resulting from the inversion over sloped terrain showed that the inversion can induce winds of this magnitude at South Pole, and suggests that this may be why the minimum temperatures and maximum inversions occur with nonzero wind speeds.

Minimum temperatures accompany winds that are blowing downslope from the higher, colder parts of the plateau. The highest temperatures occur with upslope winds, but similar temperatures are seen for a variety of unusual wind directions, which are likely caused by synoptic systems, and accompanied by clouds.

The inversion continues below 2 m, right down to the surface. In winter the median difference between the temperature at 2 m and the surface is 1.0 K, and this difference increases to 1.3 K when looking only at clear skies. The largest temperature gradient is between the surface and 20 cm, but it remains large up to 2 m.

Monthly mean temperature profiles above South Pole show large annual variations in temperature in the lower stratosphere, and the disappearance of the temperature tropopause during the polar night. They also show relatively small temperature variations in the free troposphere, and that the inversion over South Pole is much stronger and somewhat shallower than those over and around the Arctic Ocean.

A thermal-conductivity model for the snowpack, forced by downward longwave radiation, shows that the increase in downward longwave flux due to the appearance of a cloud was sufficient to explain a rapid warming event at South Pole. Light winds at the time likely reduced the role that sensible heat fluxes could play. These results support the widely held theory that the appearance of a warm cloud over the Antarctic Plateau is enough to quickly warm the surface and dramatically weaken the inversion.

Finally, a look at summer temperatures at Dome C Station showed the large effect of the diurnal cycle of

solar elevation and provided our first look at the temperature profile at this location. The inversion was destroyed during the middle of the day, and lapse conditions existed between the surface and overlying air, but at night the inversion quickly reformed. This inversion became much stronger than those seen at South Pole in summer, with an average inversion of 10 K forming after midnight between the surface and 30 m. Radiosonde data show that the effect of the diurnal cycle is limited to the lowest 150 m.

Acknowledgments. Many of the data presented in this paper were provided by NOAA's Climate Monitoring and Diagnostics Laboratory, and we are especially grateful to Thomas Mefford and Ellsworth Dutton for providing access to CMDL's data. South Pole radiosonde data were provided by the Antarctic Meteorological Research Center in Madison, Wisconsin. Paulene Roberts initiated the analyses of the tower temperatures. We also wish to thank Thomas Grenfell, Von Walden, Bradley Halter, Lance Roth, Robert Stone, and Vito Vitale for their help with the collection of the Dome C data; Delphine Six for helping erect the 32-meter tower at Dome C; and Stephen Warren, Von Walden, and Michael Town for their many helpful suggestions along the way. Stephen Warren also gave many useful comments on the first draft of this paper. This research was supported by NSF Grants OPP-97-26676, OPP-02-30466, and OPP-00-03826.

REFERENCES

Brandt, R. E., and S. G. Warren, 1993: Solar-heating rates and temperature profiles in Antarctic snow and ice. *J. Glaciol.,* **39,** 99–110.

——, and ——, 1997: Temperature measurements and heat transfer in near-surface snow at the South Pole. *J. Glaciol.,* **43,** 339–351.

Carroll, J. J., 1982: Long-term means and short-term variability of the surface energy balance components at the South Pole. *J. Geophys. Res.,* **87,** 4277–4286.

Connolley, W. M., 1996: The Antarctic temperature inversion. *Int. J. Climatol.,* **16,** 1333–1342.

Dalrymple, P. C., 1966: A physical climatology of the Antarctic Plateau. *Studies in Antarctic Meteorology,* M. J. Rubin, Ed., Antarctic Research Series, Vol. 9, Amer. Geophys. Union, 195–231.

——, H. H. Lettau, and S. H. Wollaston, 1966: South Pole micrometeorology program: Data analysis. *Studies in Antarctic Meteorology*, M. J. Rubin, Ed., Antarctic Research Series, Vol. 9, Amer. Geophys. Union, 13–57.

Davis, D., and Coauthors, 2001: Unexpected high levels of NO observed at South Pole. *Geophys. Res. Lett.,* **28,** 3625–3628.

Dozier, J., and S. G. Warren, 1982: Effect of viewing angle on the infrared brightness temperature of snow. *Water Resour. Res.,* **18,** 1424–1434.

Garratt, J. R., 1992: *The Atmospheric Boundary Layer.* Cambridge University Press, 316 pp.

Greenler, R., 1980: *Rainbows, Halos, and Glories.* Cambridge University Press, 195 pp.

Harder, S., S. G. Warren, and R. J. Charlson, 2000: Sulfate in air and snow at the South Pole: Implications for transport and deposition at sites with low snow accumulation. *J. Geophys. Res.,* **105,** 22 825–22 832.

Hogan, H. W., S. C. Barnard, and J. A. Samson, 1979: Meteorological transport of particulate material to south polar plateau. *Antarctic J. U. S.,* **14,** 192–193.

Hudson, S. R., M. S. Town, V. P. Walden, and S. G. Warren, 2004: Temperature, humidity, and pressure response of radiosondes at low temperatures. *J. Atmos. Oceanic Technol.,* **21,** 825–836.

Kahl, J. D., 1990: Characteristics of the low-level temperature inversion along the Alaskan Arctic Coast. *Int. J. Climatol.,* **10,** 537–548.

Lettau, H. H. and W. Schwerdtfeger, 1967: Dynamics of the surface-wind regime over the interior of Antarctica. *Antarct. J. U. S.,* **2,** 155–158.

Liu, H., K. Jezek, B. Li, and Z. Zhao, 2001: Radarsat Antarctic Mapping Project digital elevation model version 2. National Snow and Ice Data Center, Digital Media.

Mahesh, A., V. P. Walden, and S. G. Warren, 1997: Radiosonde temperature measurements in strong inversions: Correction for thermal lag based on an experiment at the South Pole. *J. Atmos. Oceanic Technol.,* **14,** 45–53.

——, R. Eager, J. R. Campbell, and J. D. Spinhirne, 2003: Observations of blowing snow at the South Pole. *J. Geophys. Res.,* **108,** 4707, doi:10.1029/2002JD003327.

Mahrt, L. J., and W. Schwerdtfeger, 1970: Ekman spirals for exponential thermal wind. *Bound.-Layer Meteor.,* **1,** 137–145.

Marks, R. D., 2002: Astronomical seeing from the summits of the Antarctic plateau. *Astron. Astrophys.,* **385,** 328–336.

Neff, W. D., 1999: Decadal time scale trends and variability in the tropospheric circulation over the South Pole. *J. Geophys. Res.,* **104,** 27 217–27 251.

Phillpot, H. R., and J. W. Zillman, 1970: The surface temperature inversion over the Antarctic continent. *J. Geophys. Res.,* **75,** 4161–4169.

Riordan, A. J., 1977: Variations of temperature and air motion in the 0- to 32-meter layer at Plateau Station, Antarctica. *Meteorological Studies at Plateau Station, Antarctica,* J. A. Businger, Ed., Antarctic Research Series, Vol. 25, Amer. Geophys. Union, 113–127.

Schlatter, T. W., 1972: The local surface energy balance and subsurface temperature regime in Antarctica. *J. Appl. Meteor.,* **11,** 1048–1062.

Schwerdtfeger, W., 1970a: The climate of the Antarctic. *Climates of the Polar Regions,* S. Orvig, Ed., Vol. 14, *World Survey of Climatology,* Elsevier, 253–355.

——, 1970b: Die Temperaturinversion über dem antarktischen Plateau und die Struktur ihres Windfeldes (The temperature inversion over the Antarctic Plateau and the structure of its windfield). *Meteor. Rundsch.,* **23,** 164–171.

——, 1977: Temperature regime of the South Pole: Results of 20 years' observations at Amundsen-Scott Station. *Antarctic J. U. S.,* **12,** 156–159.

——, 1984: *Weather and Climate of the Antarctic.* Elsevier, 261 pp.

Serreze, M. C., J. D. Kahl, and R. C. Schnell, 1992: Low-level temperature inversions of the Eurasian Arctic and comparisons with Soviet drifting station data. *J. Climate,* **5,** 615–629.

Solomon, S., 1990: Progress towards a quantitative understanding of Antarctic ozone depletion. *Nature,* **347,** 347–354.

Town, M. S., V. P. Walden, and S. G. Warren, 2005: Spectral and broadband longwave downwelling radiative fluxes, cloud radiative forcing and fractional cloud cover over the South Pole. *J. Climate,* in press.

Travouillon, T., M. C. B. Ashley, M. G. Burton, J. W. V. Storey, and R. F. Loewenstein, 2003: Atmospheric turbulence at the South Pole and its implications for astronomy. *Astron. Astrophys.,* **400,** 1163–1172.

Van Lipzig, N. P. M., E. Van Meijgaard, and J. Oerlemans, 2002: The effect of temporal variations in the surface mass balance and temperature-inversion strength on the interpretation of ice-core signals. *J. Glaciol.,* **48,** 611–621.

Waddington, E. D., and D. L. Morse, 1994: Spatial variations of local climate at Taylor Dome, Antarctica: Implications for paleoclimate from ice cores. *Ann. Glaciol.,* **20,** 219–225.

Walden, V. P., 1995: The downward longwave radiation spectrum over the Antarctic Plateau. Ph.D. thesis, University of Washington, 267 pp.

——, A. Mahesh, and S. G. Warren, 1996: Comment on "recent changes in the North American Arctic boundary layer in winter" by R. S. Bradley et al. *J. Geophys. Res.,* **101,** 7127–7134.

——, and Coauthors, 2001: The South Pole atmospheric radiation and cloud lidar experiment (SPARCLE). *Proc. Sixth Conf. Polar Meteorology and Oceanography,* San Diego, CA, Amer. Meteor. Soc., 297–299.

Warren, S. G., 1996: Antarctica. *Encyclopedia of Climate and Weather,* S. H. Schneider, Ed., Oxford University Press, 32–39.

Wexler, H., 1958: The "kernlose" winter in Antarctica. *Geophysica,* **6,** 577–595.

Yamanouchi, T., and S. Kawaguchi, 1984: Longwave radiation balance under a strong surface inversion in the katabatic wind zone, Antarctica. *J. Geophys. Res.,* **89,** 11 771–11 778.